

A MODEL FOR HIGH FREQUENCY QUASI-PERIODIC OSCILLATIONS FROM ACCRETING BLACK HOLES

JEREMY D. SCHNITTMAN AND EDMUND BERTSCHINGER
 Department of Physics, Massachusetts Institute of Technology
 77 Massachusetts Avenue, Cambridge, MA 02139
 schnittm@mit.edu, edbert@mit.edu
submitted to ApJ (2003)

ABSTRACT

Observations from the Rossi X-Ray Timing Explorer have shown the existence of high frequency quasi-periodic oscillations (HFQPOs) in the X-ray flux from accreting black hole binary systems. In at least two systems, these HFQPOs come in pairs with a 2:3 frequency commensurability. We propose a simple “hot spot” model to explain the position and amplitude of the HFQPO peaks. Using the exact geodesic equations for the Kerr metric, we calculate the trajectories of massive test particles, which are treated as isotropic, monochromatic emitters in their rest frames. Photons are traced from the accretion disk to a distant observer to produce time- and frequency-dependent images of the orbiting hot spot and background disk. The power spectrum of the X-ray light curve consists of multiple peaks at integral combinations of the black hole coordinate frequencies. In particular, if the radial frequency is one-third of the azimuthal frequency (as is the case near the inner-most stable circular orbit), beat frequencies appear in the power spectrum at two-thirds and four-thirds of the fundamental azimuthal orbital frequency, in agreement with observations. We also model the effects of shearing the hot spot in the disk, producing an arc of emission that also follows a geodesic orbit, as well as the effects of non-planar orbits that experience Lens-Thirring precession around the black hole axis. By varying the arc length, we are able to explain the different QPO features observed in “Type A” and “Type B” X-ray outbursts from XTE J1550-564. In the context of this model, the observed power spectra allow us to infer values for the black hole mass and angular momentum, and also constrain the parameters of the model, such as the hot spot size and luminosity.

Subject headings: black hole physics – accretion disks – X-rays:binaries

1. INTRODUCTION

In the past decade, observations of X-ray emission from accreting neutron stars and black holes have introduced new possibilities for astrophysical tests of fundamental physics. Recent discoveries made by satellites such as ASCA, RXTE, BeppoSAX, Chandra, and XMM-Newton provide direct evidence for strong-field gravitational effects in compact binary systems and active galactic nuclei (AGN). These results include Doppler-broadened iron $K\alpha$ fluorescent emission from microquasars (Miller et al. 2002) and millisecond variability of the X-ray flux from black holes in low-mass X-ray binaries (Strohmayer 2001a; Lamb 2002; Remillard et al. 2002). These measurements give the exciting prospect for determining a black hole’s mass and spin, as well as tests of general relativity in the strong-field regime.

The strong gravitational fields near a black hole (BH) introduce significant deviations from Newtonian physics, including the existence of an inner-most stable circular orbit (ISCO), a feature absent in the classical Kepler problem. Since accreting gas can efficiently lose energy and angular momentum only outside of the ISCO, the hydrodynamic and radiative behavior of the inner accretion disk should be strongly dependent on the structure of the space-time metric near the ISCO. The famous “no hair” theorem states that the only observable features of an electrically neutral black hole are functions of its mass M and specific angular momentum $a \equiv J/M$. By understanding the behavior of matter near the ISCO, we can determine the mass

and angular momentum, and thus completely describe the black hole.

Many authors have approached the problem of accretion in compact binaries with a variety of different methods, including early analytic models by Shakura & Sunyaev (1973) and Ghosh & Lamb (1978). Some have simplified the hydrodynamics in favor of a flat, thin, steady-state disk and a more detailed treatment of general relativistic effects (Laor 1991; Karas, Vokrouhlicky, & Polnarev 1992; Reynolds & Begelman 1997). To include dynamic effects, essential for modeling QPOs, others have included magnetohydrodynamics (MHD) in a pseudo-Newtonian model (Hawley & Krolik 2001; Armitage, Reynolds, & Chiang 2001) or with smoothed particle hydrodynamics (Lanzafame, Molteni, & Chakrabarti 1998; Lee & Ramirez-Ruiz 2002). A family of perturbative models has given rise to the field of diskoseismology (Wagoner, Silbergleit, & Ortega-Rodriguez 2001), where different global modes in the disk oscillate with different frequencies. Wang et al. (2003) propose a magnetic coupling between the rotating black hole and the accretion disk as a means of producing high-frequency QPOs, analogous to the Blandford-Znajek process (Blandford & Znajek 1977) used to describe AGN.

Recent observations of commensurate relationships in the high-frequency QPOs of black hole accretion disks (Remillard et al. 2002), as well as the longstanding puzzles of the frequency variability of QPO peaks and their correlations with X-ray flux and energy (Lamb 2002), motivate more detailed study of the QPO phenomenon as a means to determining the black hole parameters. We have

developed a model that is a combination of many of the above approaches in which additional physics ingredients can be added incrementally to a framework grounded in general relativity. The model does not currently include scattering, radiation pressure, magnetic fields, or hydrodynamic forces, instead treating the disk as a collection of cold test particles radiating isotropically in their respective rest frames. The trajectories of emitted photons are integrated through the metric to a distant observer to construct time-dependent images and spectra of the disk. The dynamic model uses the geodesic trajectory of a massive particle as a guiding center for a small region of excess emission, a “hot spot,” that creates a time-varying X-ray signal, in addition to the steady-state background flux from the disk.

This hot spot model is motivated by the similarity between the QPO frequencies and the black hole (or neutron star) coordinate frequencies near the ISCO (Stella & Vietri 1998, 1999) as well as the suggestion of a resonance leading to integer commensurabilities between these coordinate frequencies (Kluźniak & Abramowicz 2001, 2002). Stella & Vietri (1999) investigated primarily the QPO frequency pairs found in LMXBs with a neutron star (NS) accretor, but their basic methods can be applied to black hole systems as well.

Markovic & Lamb (2000) have presented a thorough analysis of this hot spot model for a collection of NS binaries for which pairs of QPOs have been observed. Based on a number of experimental and theoretical arguments, they conclude that the geodesic hot spot model is not a physically viable explanation for the observed NS QPOs. For low to moderate eccentricity orbits, the coordinate frequencies simply do not agree with the QPO data. For highly eccentric geodesics, they argue that the relative power in the different frequency modes are qualitatively at odds with the observations. Furthermore, they show that hydrodynamical considerations place strong constraints on the possible size, luminosity, coherency, and trajectories of the hot spots.

Many of these points are addressed in our version of the hot spot model. Also, by including full 3-dimensional (3D) ray-tracing, we can quantitatively predict how much QPO power will be produced by a hot spot of a given size and emissivity moving along a geodesic orbit near the ISCO. Along with the special relativistic beaming of the emitted radiation, we find that strong gravitational lensing can cause high-amplitude modulations in the light curves, even for relatively small hot spots. The issues of differential rotation and shearing of the emission region are addressed below when we consider the generalization of the hot spot model to include arcs and non-planar geometries.

Perhaps the most powerful feature of this hot spot model is the facility with which it can be developed and extended to more general accretion disk geometries. In addition to providing a possible explanation for the commensurate HFQPOs in at least two systems (XTE J1550-564 and GRO J1655-40), the hot spot model with full general relativistic ray-tracing is a useful building block toward any other viable model of a dynamic 3D accretion disk. Within the computational framework of the Kerr metric, we can investigate many different emission models and compare their predicted X-ray spectra and light curves with obser-

vations. For example, our ray-tracing code could be used in conjunction with a 3D MHD calculation of the accretion disk to simulate the time-dependent X-ray flux and spectrum from such a disk.

It is with this motivation that we present the initial results of the model. Section 2 describes the relativistic ray-tracing methods and discusses numerical techniques. In Section 3, we develop the basic model of a steady-state disk with the potential application to broad iron $K\alpha$ emission. Section 4 introduces the basic hot spot model for circular geodesics and shows the effect of binary inclination and black hole spin on the QPO power spectrum. In Section 5 the model is extended to trajectories with non-zero eccentricity and inclination, as well as elongated hot spots or arcs, giving a set of model parameters that best fit the QPO data from a large number of outbursts from XTE J1550-564. In Section 6 we present our conclusions and a discussion of future work.

2. RAY-TRACING IN THE KERR METRIC

We begin by dividing the image plane into regularly spaced “pixels” of equal solid angle in the observer’s frame, each corresponding to a single ray. Following the sample rays backward in time, we calculate the original position and direction that a photon emitted from the disk would require in order to arrive at the appropriate position in the detector. The gravitational lensing and magnification of emission from the plane of the accretion disk is performed automatically by the geodesic integration of these evenly spaced photon trajectories, so that high magnification occurs in regions where nearby points in the disk are projected to points with large separation in the image plane. To model the time-varying emission from the disk, each photon path is marked with the time delay along the path from the observer to the emission point in the disk.

To integrate the geodesic trajectories of photons or massive particles, we use a Hamiltonian formalism that takes advantage of certain conserved quantities in the dynamics. The resulting equations of motion do not contain any sign ambiguities from turning points in the orbits, as are introduced by many classical treatments of the geodesic equations in the Kerr metric. We define a Hamiltonian function of eight phase space variables (x^ν, p_μ) and an integration variable (affine parameter) λ along the path length. For a general space-time metric $g_{\mu\nu}(\mathbf{x})$ with inverse $g^{\mu\nu}(\mathbf{x})$, we can define a Hamiltonian H_2 quadratic in the momenta as

$$H_2(x^\mu, p_\nu; \lambda) = \frac{1}{2}g^{\mu\nu}(\mathbf{x})p_\mu p_\nu = -\frac{1}{2}m^2, \quad (1)$$

where the rest mass m is a constant ($m = 0$ for photons, $m = 1$ for massive particles).

Applying Hamilton’s equations from classical mechanics, we reproduce the geodesic equations:

$$\frac{dx^\mu}{d\lambda} = \frac{\partial H_2}{\partial p_\mu} = g^{\mu\nu}p_\nu = p^\nu, \quad (2a)$$

$$\frac{dp_\mu}{d\lambda} = -\frac{\partial H_2}{\partial x^\mu} = -\frac{1}{2}\frac{\partial g^{\alpha\beta}}{\partial x^\mu}p_\alpha p_\beta = g^{\gamma\beta}\Gamma_{\mu\gamma}^\alpha p_\alpha p_\beta. \quad (2b)$$

For any metric, the Hamiltonian H_2 is independent of the affine parameter λ , allowing us to use one of the coordinates as the integration parameter and reduce the dimensionality of the phase space by two. We use the coordinate

$t = x^0$ as the time coordinate for the six dimensional phase space (x^i, p_i) . The corresponding Hamiltonian is

$$H_1(x^i, p_i; t) \equiv -p_0 = \frac{g^{0i}p_i}{g^{00}} + \left[\frac{g^{ij}p_i p_j + m^2}{-g^{00}} + \left(\frac{g^{0i}p_i}{g^{00}} \right)^2 \right]^{1/2} \quad (3)$$

with equations of motion

$$\frac{dx^i}{dt} = \frac{\partial H_1}{\partial p_i}, \quad (4a)$$

$$\frac{dp_i}{dt} = -\frac{\partial H_1}{\partial x^i}. \quad (4b)$$

We have thus reduced the phase space to the six-dimensional tangent bundle (x^i, p_i) . Moreover, because the metric is independent of $t = x^0$, $H_1 = -p_0$ is also an integral of motion.

In Boyer-Lindquist coordinates (t, r, θ, ϕ) , the Kerr metric may be written

$$ds^2 = -\alpha^2 dt^2 + \varpi^2 (d\phi - \omega dt)^2 + \frac{\rho^2}{\Delta} dr^2 + \rho^2 d\theta^2, \quad (5)$$

which allows a relatively simple form of the inverse metric

$$g^{\mu\nu} = \begin{pmatrix} -1/\alpha^2 & 0 & 0 & -\omega/\alpha^2 \\ 0 & \Delta/\rho^2 & 0 & 0 \\ 0 & 0 & 1/\rho^2 & 0 \\ -\omega/\alpha^2 & 0 & 0 & 1/\varpi^2 - \omega^2/\alpha^2 \end{pmatrix}. \quad (6)$$

For a black hole of mass M and specific angular momentum $a = J/M$, we define (in geometrized units with $G = c = 1$)

$$\rho^2 \equiv r^2 + a^2 \cos^2 \theta \quad (7a)$$

$$\Delta \equiv r^2 - 2Mr + a^2 \quad (7b)$$

$$\alpha^2 \equiv \frac{\rho^2 \Delta}{\rho^2 \Delta + 2Mr(a^2 + r^2)} \quad (7c)$$

$$\omega \equiv \frac{2Mra}{\rho^2 \Delta + 2Mr(a^2 + r^2)} \quad (7d)$$

$$\varpi^2 \equiv \left[\frac{\rho^2 \Delta + 2Mr(a^2 + r^2)}{\rho^2} \right] \sin^2 \theta. \quad (7e)$$

As a check, we see that the metric reduces to the well-known Schwarzschild metric in the limit $a \rightarrow 0$. In the limit $M \rightarrow 0$, it reduces to flat space-time with hyperbolic-elliptical coordinates.

With this form of the metric, the Hamiltonian H_1 can be written

$$H_1(r, \theta, \phi, p_r, p_\theta, p_\phi; t) = \omega p_\phi + \alpha \left(\frac{\Delta}{\rho^2} p_r^2 + \frac{1}{\rho^2} p_\theta^2 + \frac{1}{\varpi^2} p_\phi^2 + m^2 \right) \quad (8)$$

This new Hamiltonian is also independent of ϕ (azimuthally symmetric space-time), giving the conjugate momentum p_ϕ as the second integral of motion for H_1 . We are now left with five coupled equations for $(r, \theta, \phi, p_r, p_\theta)$. The third integral of motion, Carter's constant (Carter 1968)

$$\mathcal{Q} \equiv p_\theta^2 + \cos^2 \theta [a^2(m^2 - p_0^2) + p_\phi^2 / \sin^2 \theta], \quad (9)$$

is used as an independent check of the accuracy of the numerical integration.

As mentioned above, many traditional schemes to calculate trajectories in the Kerr metric use this additional

integral of motion to further reduce the dimensionality of the problem (Misner, Thorne, & Wheeler 1973) and even reduce the problem to one of quadrature integration [e. g. Rauch & Blandford (1994)]. While potentially increasing the speed of the computation, this approach also introduces significant complications in the form of arbitrary signs in the equations of motion corresponding to turning points in r and θ . Another common approach is to define effective potentials in $U_{\text{eff}}(r)$ and $V_{\text{eff}}(\cos \theta)$, which give a set of four parametric equations for $r(\lambda), \theta(\lambda), \phi(\lambda)$, and $t(\lambda)$. These parametric solutions introduce the difficulty of reconstructing the coordinate momenta, which are not evolved along with the coordinate positions. In our ray-tracing algorithm, we have traded a modest improvement in computational speed for simplicity in implementation.

The initial conditions for the photon or particle geodesics are determined in the local orthonormal frame of a ‘‘Zero-Angular Momentum Observer’’ (ZAMO). The ZAMO basis is defined such that the spatial axes are aligned with the coordinate axes and then the time axis is determined by orthogonality (Bardeen, Press, & Teukolsky 1972). The ZAMO tetrad \mathbf{e}_μ is

$$\mathbf{e}_t = \frac{1}{\alpha} \mathbf{e}_t + \frac{\omega}{\alpha} \mathbf{e}_\phi \quad (10a)$$

$$\mathbf{e}_r = \sqrt{\frac{\Delta}{\rho^2}} \mathbf{e}_r \quad (10b)$$

$$\mathbf{e}_\theta = \sqrt{\frac{1}{\rho^2}} \mathbf{e}_\theta \quad (10c)$$

$$\mathbf{e}_\phi = \sqrt{\frac{1}{\varpi^2}} \mathbf{e}_\phi, \quad (10d)$$

where \mathbf{e}_μ is the standard coordinate basis in Boyer-Lindquist coordinates. One advantage of the ZAMO basis is that the basis vector \mathbf{e}_t is time-like ($g_{tt} < 0$) everywhere outside of the horizon. For a coordinate stationary observer, on the other hand, the time basis vector \mathbf{e}_t becomes space-like ($g_{tt} > 0$) inside the ergosphere $r_{\text{erg}} = M + \sqrt{M^2 - a^2 \cos^2 \theta}$. For sufficiently large values of the spin parameter a , the inner-most stable circular orbit (often taken for the inner edge of the accretion disk) extends within the ergosphere, emphasizing the advantage of using the ZAMO basis.

At a point far away from the black hole, the space-time is nearly flat so Euclidean spherical geometry gives the spatial direction of the photon $n^i \mathbf{e}_i$, from which the initial momentum in the coordinate basis is calculated:

$$p_t = -E_{\text{obs}}(\omega \varpi n^\phi + \alpha) \quad (11a)$$

$$p_r = E_{\text{obs}} \sqrt{\frac{\rho^2}{\Delta}} n^r \quad (11b)$$

$$p_\theta = E_{\text{obs}} \sqrt{\rho^2} n^\theta \quad (11c)$$

$$p_\phi = E_{\text{obs}} \sqrt{\varpi^2} n^\phi, \quad (11d)$$

where the photon energy measured by the distant ZAMO is E_{obs} .

The photon trajectories are integrated backward in time from the image plane oriented at some inclination angle i with respect to the axis of rotation for the black hole, where $i = 0^\circ$ corresponds to a face-on view of the disk and $i = 90^\circ$ is an edge-on view. The accretion disk is confined

to a finite region of latitude with angular thickness $\Delta\theta$ normal to the rotation axis. The photons terminate either at the event horizon or pass through the surfaces of colatitude $\theta = \text{const}$, as shown in Figure 1. As trajectories pass through the disk, the photon’s position and momentum (x^μ, p_μ) are recorded for each plane intersection in order to later reconstruct an image of the disk.

For an infinitely thin disk ($\Delta\theta \rightarrow 0$), it is easy to show how the image plane maps onto the source plane. Taking an evenly spaced grid of initial photon directions, Figure 2 shows the positions of intersection with the source plane, in pseudo-Cartesian coordinates defined by

$$\begin{aligned} x &= \sqrt{r^2 + a^2} \cos \phi \\ y &= \sqrt{r^2 + a^2} \sin \phi. \end{aligned} \quad (12)$$

Photons that cross the black hole event horizon before intersecting the plane are not shown. As the rays are deflected by the black hole, they tend to be focused on the far side, giving a strong magnification by mapping a large area in the image plane onto a small area of the source plane, as seen here by a higher density of lattice grid points. For the flat disk geometry, rays are not allowed to pass through the plane defined by $\theta = 0$, so we do not see multiple images of sources “behind” the black hole, as is often observed in the strong gravitational lensing of distant quasars by intervening galaxies. However, for sufficiently high inclinations and spin values, single points in the equatorial plane can be mapped to different regions of the image plane, creating multiple images of certain regions of the disk. This effect is seen in the folding of the image map onto itself near the horizon in the bottom right of Figure 2.

The disk itself is modeled as a collection of mass elements moving along circular geodesics around the black hole, emitting isotropic, monochromatic light with energy E_{em} in the emitter’s rest frame. For each photon with 4-momentum $p_\mu(\mathbf{x}_{\text{em}})$ intersecting a particle trajectory with coordinate velocity $v^\mu(\mathbf{x}_{\text{em}})$, the measured redshift is given by

$$\frac{E_{\text{obs}}}{E_{\text{em}}} = \frac{p_\mu(\mathbf{x}_{\text{obs}})v^\mu(\mathbf{x}_{\text{obs}})}{p_\mu(\mathbf{x}_{\text{em}})v^\mu(\mathbf{x}_{\text{em}})}, \quad (13)$$

where for a distant observer at $r \rightarrow \infty$, we take $v^\mu(\mathbf{x}_{\text{obs}}) = [1, 0, 0, 0]$.

For disk models with finite thickness, the radiation transport equation can be solved as the ray passes through the disk. In a locally flat frame, the radiation transport equation is

$$\frac{dI_\nu}{ds} = j_\nu - \kappa_\nu I_\nu, \quad (14)$$

where ds is the differential path length and I_ν , j_ν , and κ_ν are respectively the radiation intensity and the emissivity and opacity of the plasma at a frequency ν (scattering terms can be included in both j_ν and κ_ν). Additionally, as the photon bundle propagates through the global curvature around the black hole, the spectral intensity at a given frequency evolves as the photons are gravitationally red-shifted, maintaining the Lorentz invariance of I_ν/ν^3 .

For most of the calculations presented in this paper, we are primarily concerned with radiation coming from a limited region of the disk, treated as a monochromatic source with $\kappa_\nu = 0$ and $j_\nu(\mathbf{x}) = \delta(\nu - \nu_{\text{em}})g(\mathbf{x})$, with $g(\mathbf{x})$ the emissivity at space-time coordinate \mathbf{x} . When calculating the emission from a flat, steady-state disk, the

plane defined by $\cos\theta = 0$ is taken to be totally opaque [$g(\mathbf{x}) \propto \delta(\cos\theta)$; $\kappa_\nu(\cos\theta < 0) \rightarrow \infty$] so that rays cannot curve around and see the “underside” of the accretion disk. For each pixel (i, j) in the image plane, an observed photon bundle spectrum $I_\nu(t_{\text{obs}}, i, j)$ is given for each time step by integrating the contribution of the hot spot and the disk through the computational grid. This collection of incident photons can then be summed to give time-dependent light curves, spectra, or spatially resolved images. The results of this paper are based primarily on flat, steady state disks and single hot spots, yet with the computational methods described above, arbitrary disk geometries and emissivity/opacity models can be simulated as well.

The ray-tracing calculation is carried out by numerically integrating equations (4a) and (4b) with a fifth-order Runge-Kutta algorithm with adaptive time stepping. This provides high accuracy over a large range of scales as the photon follows a long path through the relatively flat space-time between the observer and the black hole, and then experiences strong curvature over a small region close to the horizon. We typically maintain an accuracy of one part in 10^{11} , which can be independently confirmed by monitoring \mathcal{Q} , Carter’s constant. The images and spectra are formed by ray-tracing a set of photon paths, usually of the order 400×400 grid points in (i, j) with ~ 20 latitudinal zones in θ and spectral resolution of $\nu/\Delta\nu \sim 200$.

3. SPECTRA FROM STEADY-STATE DISKS

A steady-state disk can be made of a collection of massive particles moving in concentric planar circular orbits. For orbits at a radius r in a plane orthogonal to the spin axis, a particle’s specific energy and angular momentum are given analytically by Shapiro & Teukolsky (1983):

$$-p_0 = \frac{r^2 - 2Mr \pm a\sqrt{Mr}}{r(r^2 - 3Mr \pm 2a\sqrt{Mr})^{1/2}} \quad (15)$$

and

$$p_\phi = \pm \frac{\sqrt{Mr}(r^2 \mp 2a\sqrt{Mr} + a^2)}{r(r^2 - 3Mr \pm 2a\sqrt{Mr})^{1/2}}. \quad (16)$$

Here the top sign is taken for prograde orbits (particle angular momentum parallel to black hole angular momentum) and the bottom sign for retrograde orbits. Inside the ISCO, the particles follow plunge trajectories with constant energy and angular momentum determined at the ISCO. In practice, when calculating emission from a steady-state disk, we take the inner edge of the disk to be the ISCO radius R_{ISCO} .

For a disk made up of massive particles on circular orbits emitting isotropically from a region between R_{in} and R_{out} , the Doppler broadening of an emission line (typically iron $K\alpha$ with $E_{\text{em}} \approx 6.5$ keV) may be used to determine the inclination of the disk with respect to the observer. Disks at higher inclination will have an intense blue-shifted segment of the spectrum corresponding to the Doppler-boosted photons emitted from gas moving toward the observer. The higher intensity for the blue-shifted photons is caused by relativistic beaming, determined by the Lorentz invariance of I_ν/ν^3 along a photon bundle:

$$I_\nu(\text{obs}) = I_\nu(\text{em}) \frac{\nu_{\text{obs}}^3}{\nu_{\text{em}}^3}. \quad (17)$$

Figure 3 shows the integrated spectra from a set of accretion disks with outer radius $R_{\text{out}} = 15M$ and inner radius at $R_{\text{in}} = R_{\text{ISCO}}$ for a spin parameter $a/M = 0.5$, normalized such that $\int I(E_{\text{obs}}/E_{\text{em}})d(E_{\text{obs}}/E_{\text{em}}) = 1$. All spectra are assumed to come from a flat, opaque disk with uniform emission [$g(\mathbf{x}) \propto \delta(\cos \theta)$]. Repeating this calculation for a range of spin parameters (and thus a range of R_{ISCO}), we find that the dependence on disk inclination is quite strong, while the dependence on black hole spin is almost insignificant. This is reasonable because, except for very close to the horizon, the spin has little effect on the orbital velocity for circular orbits: for spin parameter a and radius r , the observed angular frequency is given by

$$\Omega_{\phi} = \frac{\pm\sqrt{M}}{r^{3/2} \pm a\sqrt{M}}, \quad (18)$$

where again we take the upper sign for prograde orbits and the lower sign for retrograde orbits. For the large part of the disk, the orbits have nearly Keplerian orbital frequencies, as measured in coordinate time t . For larger values of a , the ISCO extends in close to the event horizon, increasing the radiative area of the disk. However, due to the strong gravitational redshift in this inner region, the observed intensity is reduced by a significant factor of $\nu_{\text{obs}}^3/\nu_{\text{em}}^3$, resulting in a weak dependence on spin for disks with uniform emission.

Many accretion disk models include an emissivity that scales as a power of the radius. Following Bromley, Chen, & Miller (1997), we apply an emissivity factor proportional to r^{-2} , giving an added weight to the inner, presumably hotter, regions. For the inner section of an accretion disk with $R_{\text{out}} = 15M$, this inverse-square dependence closely approximates the classic Shakura-Sunyaev steady-state disk model (Shakura & Sunyaev 1973).

As can be seen in Figure 4, this extra emission from close to the black hole serves to break the otherwise weak dependence on spin. For an inclination of $i = 30^\circ$, five different spin values are shown: ($a/M = -0.99, -0.5, 0, 0.5, 0.99$), corresponding to inner disk boundaries at ($R_{\text{ISCO}}/M = 8.97, 7.55, 6.0, 4.23, 1.45$). Since the sign of a is defined with respect to the angular momentum of the accretion disk, negative values of a imply retrograde orbits that do not survive as close to the black hole, plunging at larger values of R_{ISCO} . The disks that extend in closer produce more low-energy red-shifted photons, giving longer tails to the spectra at $E_{\text{obs}}/E_{\text{em}} < 0.7$ and smaller relative peaks at $E_{\text{obs}}/E_{\text{em}} \approx 1$.

Thus, if we can determine the inclination of the disk independently (e.g. through spectroscopic observations of the binary companion), the spin may be inferred from the broadening of an iron emission line. However, since the plane of the disk tends to align normal to the black hole spin axis close to the ISCO, the binary inclination may not coincide with the inclination of the inner disk. The problem of inclination, along with other complications, such as additional emission lines and other causes of scattering and line broadening, motivates us to look more closely at the QPO spectra as a method for determining black hole spin.

4. HOT SPOT EMISSION

Given the map from the accretion disk to the image plane, with each photon bundle labeled with a distinct

4-momentum and time delay, we can reconstruct time-dependent images of the disk based on time-varying emission models. The simplest model we consider is a single region of isotropic, monochromatic emission following a geodesic trajectory: the “hot spot” or “blob” model (Stella & Vietri 1998, 1999).

The hot spot is a small region with finite radius and emissivity chosen to have a Gaussian distribution in local Cartesian space:

$$g(\mathbf{x}) \propto \exp\left[-\frac{|\tilde{\mathbf{x}} - \tilde{\mathbf{x}}_{\text{spot}}(t)|^2}{2R_{\text{spot}}^2}\right]. \quad (19)$$

The spatial position 3-vector $\tilde{\mathbf{x}}$ is given in pseudo-Cartesian coordinates by the transformation defined by equation (12) and $z = r \cos \theta$. Outside a distance of $4R_{\text{spot}}$ from the guiding geodesic trajectory, there is no emission. We typically take $R_{\text{spot}} = 0.25 - 0.5M$, but find the normalized light curves and QPO power spectra to be independent of spot size. Because we assume all points in the hot spot have the same 4-velocity as the geodesic guiding trajectory, one must be careful not to use too large a spot or the point of emission \mathbf{x} can be spatially far enough away from the center \mathbf{x}_{spot} to render the inner product $p_{\mu}(\mathbf{x})v^{\mu}(\mathbf{x}_{\text{spot}})$ unphysical. We have also explored a few different hot spot shapes, ranging from spherical to a disk flattened in the $\hat{\theta}$ direction and similarly find no significant dependence of the spectra on spot shape.

After calculating and tabulating the hot spot trajectory as a function of coordinate time t , the ray-tracing map between the disk and the observer is used to construct a time-dependent light curve from the emission region. For each photon bundle intersection point there is a time delay $\Delta t_{i,j,k}$ (where i, j are the coordinate indices in the image plane and k is the latitude index in the disk) so for the observer time t_{obs} , we first determine where the hot spot was at coordinate time $(t_{\text{em}})_{i,j,k} = t_{\text{obs}} - \Delta t_{i,j,k}$. If the spot centroid is close (within $4R_{\text{spot}}$) to the disk intersection point $(r, \theta, \phi)_{i,j,k}$, then the redshifted emission is added to the pixel spectrum $I_{\nu}(t_{\text{obs}}, i, j)$, weighted by equation (19).

In this way, a movie can be produced that shows the blob orbiting the black hole, including all relativistic effects. Such a movie shows a few immediately apparent special relativistic effects such as the Doppler shift and beaming as the spot moves toward and then away from the observer. For a hot spot orbiting in the clock-wise direction as seen from above ($v^{\phi} < 0$ with $\phi = 270^\circ$ toward the observer), the point of maximum blue shift actually occurs at a point where $\phi > 0$ because of the gravitational lensing of the light, beamed in the forward direction of the emitter and then bent toward the observer by the black hole. Gravitational lensing also causes significant magnification of the emission region when it is on the far side of the black hole, spreading the image into an arc, much like distant galaxies are distorted by intervening matter in galaxy clusters.

A simulated time-dependent spectrum or *spectrogram* for this hot spot model is shown in Figure 5. The horizontal axis measures time in the observer’s frame, with $t = 0$ corresponding to the time at which the spot center is moving most directly away from the observer ($\phi = 180^\circ$). As mentioned above, this is *not* the same as the point of

maximum redshift, which occurs closer to $\phi = 160^\circ$ due to gravitational deflection of the emitted light.

The spectrum shown in Figure 5 can be integrated in time to give a spectrum similar to those shown in Figures 3 and 4, corresponding to something like a very narrow circular emitting region with $R_{\text{out}} \approx R_{\text{in}} \approx R_{\text{ISCO}}$. By integrating over frequency, we get the total X-ray flux as a function of time, i.e. the light curve $I(t)$. This time-varying signal can be added to a background intensity coming from the inner regions of a steady state disk described in Section 3. By definition the hot spot will have a higher temperature or density and thus greater emissivity than the background disk, adding a small modulation to the total flux. RXTE observations find the HFQPO X-ray modulations to have typical amplitudes of 1-5% of the mean flux during the outburst (Remillard et al. 2002). Markovic & Lamb (2000) present a first-order argument that a 1% amplitude modulation requires a hot spot with 100% overbrightness extending over an area of 1% of the steady-state region of the disk. For $R_{\text{out}} = 15M$, this requires a hot spot with radius $R_{\text{spot}} \approx 1.5M$, which they argue is too large to survive the viscous shearing of the disk.

Hydrodynamic stability aside, this reasoning ignores the important effects of disk inclination, relativistic beaming and gravitational lensing of the hot spot emission. Also, assuming a Shakura-Sunyaev type disk with steady-state emissivity $g(r) \propto r^{-2}$ and a similar scaling for the hot spot emission, we find that hot spots with smaller size and overbrightness are capable of creating X-ray modulations on the order of 1% rms, defined by

$$\text{rms} \equiv \sqrt{\frac{\int [I(t) - \bar{I}]^2 dt}{\int I(t) dt}}. \quad (20)$$

Figure 6 shows the required overbrightness of a flattened Gaussian hot spot orbiting near the ISCO to produce a modulation with rms amplitude of 1% for a range of inclinations and black hole spin parameters. In the limit of a face-on accretion disk ($i = 0^\circ$), even an infinitely bright spot on a circular orbit will not produce a time-varying light curve. As the inclination increases, the required overbrightness decreases, as the special relativistic beaming focuses radiation toward the observer from a smaller region of the disk, *increasing* the relative contribution from the hot spot. As the spin of the black hole increases, the ISCO moves in toward the horizon and the velocity of a trajectory near that radius increases, as does the gravitational lensing, magnifying the contribution from the hot spot.

Understandably, the required overbrightness is inversely proportional to the area of the hot spot so [overbrightness] * $R_{\text{spot}}^2 = \text{const}$. For example, from Figure 6 we see that a black hole binary with inclination $i = 60^\circ$ and spin $a/M = 0.5$ would require a spot size of $R_{\text{spot}} = 0.5M$ with 67% overbrightness (e.g. 14% temperature excess) to produce a 1% rms modulation in the light curve. This is well within the range of the typical size and magnitude of fluctuations predicted by 3D MHD calculations of 3-dimensional accretion disks (Hawley & Krolik 2001). The hot spot model is well-suited for simplified calculations of the X-ray emission from these random fluctuations in the accretion disk. By adding the emission from small, coherent hot spots to a steady-state Shakura-

Sunyaev disk, we can interpret the amplitudes and positions of features in the QPO spectrum in terms of a model for the black hole mass, spin, and inclination.

Considering the X-ray flux from the hot spot alone, the frequency-integrated light curves for a variety of inclinations are shown in Figure 7. All light curves are shown for one period of a hot spot orbiting a Schwarzschild black hole at the ISCO. As the inclination increases, the light curve goes from nearly sinusoidal to being sharply peaked by special relativistic beaming. Thus the shape of a QPO light curve may be used to determine the disk inclination. With current observational capabilities, it is not possible even for the brightest sources to get a strong enough X-ray signal over individual periods as short as 3-5 ms to be able to differentiate between the light curves in Figure 7. Instead, the Fourier power spectrum can be used to identify the harmonic features of a periodic or quasi-periodic light curve over many orbits. Disks with higher inclinations will give more power in the higher harmonic frequencies, due to the ‘‘lighthouse’’ effect, as the hot spot shoots a high-power beam of photons toward the observer once per orbit, approximating a periodic delta-function in time.

Figure 8a shows a sample section of such a light curve, including only the X-ray flux from the hot spot, subtracting out the steady-state flux from the disk. The sharp peaks in the light curve, while unresolvable in the time domain, will give a characteristic amount of power in the higher harmonics, shown in Figure 8b. Here we have normalized the rms amplitudes to the background flux from the disk with a hot spot overbrightness of 100 %. For a signal $I(t)$ with Fourier components a_n :

$$I(t) = \sum_{n=0}^{\infty} a_n \cos(2\pi n t), \quad (21)$$

we define the rms amplitude $a_n(\text{rms})$ in each mode $n > 0$ as

$$a_n(\text{rms}) \equiv \frac{a_n}{\sqrt{2a_0}}. \quad (22)$$

With this normalization, the rms defined in equation (20) can be conveniently written

$$\text{rms} = \sqrt{\sum_{n>0} a_n^2(\text{rms})}. \quad (23)$$

In Figure 8b, the main peak at $f = 220$ Hz corresponds to the fundamental azimuthal frequency for an orbit at the ISCO of a $10M_\odot$ Schwarzschild black hole. In the limit where the light curve is a periodic delta-function in time, there should be an equal amount of power in all harmonic modes, because the Fourier transform of a periodic delta-function is a periodic delta-function. However, even in the limit of edge-on inclination ($i = 90^\circ$), unless the hot spot is infinitesimally small and ultra-relativistic, the light curve will always be a continuous function with some finite width and non-zero minimum, thus contributing less and less power to the higher harmonics. The harmonic dependence on inclination for a hot spot orbiting a Schwarzschild black hole is shown in Figure 9. Predictably, as the inclination increases, we see that both the absolute and relative amplitudes of the higher harmonics increase, almost to the limit of a periodic delta-function when $i \rightarrow 90^\circ$. Interestingly, we find very little dependence of the harmonic structure on hot spot size or shape,

as long as the total emission of the spot relative to the disk is constant (this emphasizes the robustness of the simple hot spot model in interpreting an X-ray power spectrum, without needing to include the detailed physics of the disk perturbations).

As the spin parameter increases for Kerr black holes, the ISCO moves closer to the horizon, increasing the circular velocities of particles on the ISCO and thus the Doppler shifts, giving broader time-integrated spectra, as seen in Figure 4. The phase lag in time of the peak blueshift with respect to angular phase of the hot spot is also amplified for these smaller values of R_{ISCO} , giving light curves that are asymmetric in time. The hot spot orbits around Kerr black holes also experience more gravitational lensing as they move through the strongly curved space-time near the horizon. This lensing becomes more significant for larger inclinations as the black hole and the emitting region approach collinearity with the observer, producing an Einstein ring as $i \rightarrow 90^\circ$. This somewhat counters the special relativistic beaming effect as the light curve peaks over a broader phase of each period due to lensing. Thus the harmonic power dependence on inclination for a Kerr light curve is in fact smaller than that for the Schwarzschild geometry. However, in the event that the accretion disk is actually rotating in a retrograde fashion with respect to the black hole spin, the ISCO will move *away* from the horizon [$R_{\text{ISCO}}(a/M = -0.99) = 8.97M$], reversing the above effects and giving a *stronger* dependence on inclination.

5. NON-CIRCULAR ORBITS

One of the major unsolved puzzles motivating theoretical models of black hole QPOs is the observation of multiple peaks in the high frequency power spectrum (Lamb 2002). As discussed above, any non-sinusoidal light curve will contribute to Fourier power in harmonics at integer multiples of the fundamental Kepler frequency. However, for at least two X-ray binary systems (XTE J1550-564 and GRO J1655-40; possibly also GRS 1915+105), peaks are found with rational (but non-integer) frequency ratios (Strohmayer 2001b; Remillard et al. 2002). In these particular examples, significant power is measured around the frequencies (184, 276 Hz) for XTE J1550-564 and (300, 450 Hz) for GRO J1655-40, almost exactly a 2:3 commensurability in frequencies, while GRS 1915+105 has peaks at 40 and 67 Hz. Following the work of Merloni, Vietri, & Stella (1999), we investigate the possibility of these commensurabilities coming from integral combinations of the radial and azimuthal coordinate frequencies of nearly circular geodesics around a Kerr black hole.

In a Newtonian point mass potential, the radial, azimuthal, and vertical (latitudinal) frequencies ν_r , ν_ϕ , and ν_θ are identical, giving closed planar elliptical orbits. For the Schwarzschild metric the vertical and azimuthal frequencies are identical, giving planar rosette orbits that are closed only for a discrete set of initial conditions. The Kerr metric allows three unique coordinate frequencies, so geodesic orbits in general can fill out a torus-shaped region around the black hole spin axis. When these coordinate frequencies are rational multiples of each other, the trajectories will close after a finite number of orbits.

While there is currently no clear physical explanation for

why hot spots may tend toward such trajectories, some recent evidence suggests the possible existence of nonlinear resonances near geodesic orbits with integer commensurabilities (Abramowicz et al. 2003). Another important clue may come from the fact that at these special orbits are closed, perhaps enhancing the stability of non-circular trajectories. The quasi-periodic nature of the oscillations suggest the continual formation and subsequent destruction of hot spots *near*, but not exactly at, the resonant orbits. For the purposes of this paper, we will take the apparent preference for such orbits as given and concern ourselves primarily with calculating the resulting light curves and power spectra.

In geometrized units with $G = c = M = 1$, coordinate time is measured in units of $4.9 \times 10^{-6}(M/M_\odot)$ sec. For example, an orbit with angular frequency $\Omega_\phi = 2\pi\nu_\phi = 0.1$ around a $10M_\odot$ black hole would have an observed period of 3.1 ms, whereas the analogous orbit around a supermassive black hole with mass 10^9M_\odot would have a period of 8.6 hours. In these units, the three fundamental coordinate frequencies for nearly circular orbits are given by equation (18) and (Merloni, Vietri, & Stella 1999)

$$\Omega_\theta = 2\pi\nu_\theta = \Omega_\phi \left[1 \mp \frac{4a}{r^{3/2}} + \frac{3a^2}{r^2} \right]^{1/2} \quad (24)$$

and

$$\Omega_r = 2\pi\nu_r = \left[\frac{r^2 - 6r \pm 8ar^{1/2} - 3a^2}{r^2(r^{3/2} \pm a)^2} \right]^{1/2}, \quad (25)$$

where the upper sign is taken for prograde orbits and the lower sign is taken for retrograde orbits. The radial frequency approaches zero at $r \rightarrow R_{\text{ISCO}}$, where geodesics can orbit the black hole many times with steadily decreasing r . In the limit of zero spin and large r , the coordinate frequencies reduce to the degenerate Keplerian case with $\Omega_\phi = \Omega_\theta = \Omega_r = r^{-3/2}$.

To model the 2:3 frequency commensurability, we begin by looking for perturbed circular planar orbits where the radial frequency ν_r is one-third the azimuthal frequency ν_ϕ . Since the orbits are nearly circular, the fundamental mode of the light curve should peak at the azimuthal frequency with additional power in beat modes at $\nu_\phi \pm \nu_r$. For $\nu_r:\nu_\phi = 1:3$, the power spectrum should have a triplet of peaks with frequency ratios 2:3:4. These commensurate orbits can be found easily from equations (18) and (25) and solving for r :

$$r^2 - 6r \pm 8ar^{1/2} - 3a^2 = \pm \frac{r^2}{9}(r^{3/2} \pm a). \quad (26)$$

Figure 10 shows the radius (solid lines) of these special orbits as a function of spin parameter. Also shown (dashed line) is the inner-most stable circular orbit for prograde trajectories. The position of the 1:3 commensurate orbits follows closely outside the ISCO, suggesting a connection between the high frequency QPOs and the black hole ISCO. However, other integer commensurabilities such as 1:2, 2:5, or 1:4 also closely follow the ISCO curves for varying a , so the proximity to the ISCO alone is probably not enough to explain the hot spot preference for these specific coordinate frequencies. It is important to note that any given black hole source will have a constant value of a , certainly over the lifetime of our observations. Thus, we may need to observe many more sources like XTE J1550-564

and GRO J1655-40 in order to better sample the parameter space of Figure 10 and thus the connection between certain preferred orbits and the black hole ISCO.

A 1:3 commensurate trajectory moves through three revolutions in azimuth for each radial period, forming a closed rosette of three “layers.” For such rosettes, the eccentricity can be defined as

$$e \equiv \frac{r_{max} - r_{min}}{r_{max} + r_{min}}. \quad (27)$$

The time-dependent light curve for a prograde orbit with eccentricity $e = 0.089$, spin $a/M = 0.5$, and inclination $i = 60^\circ$ is shown in Figure 11a. The time axis begins at the point when the hot spot is at apocenter, moving away from the observer. Thus the first and third peaks come from the hot spot moving toward the observer at a relatively larger radius, while the second, higher peak is caused by the emitter moving toward the observer through pericenter at a higher velocity, giving a larger blue-shift and thus beaming factor. The combined Doppler beaming and gravitational lensing causes the peak following the pericenter peak to be slightly larger, as the emitter is moving away from the black hole yet the light is focused more toward the observer.

The power spectrum for this light curve is shown in Figure 11b, with the strongest peaks at the azimuthal frequency of $\nu_\phi = 285$ Hz and its first harmonic at $2\nu_\phi = 570$ Hz for $M = 10M_\odot$. Even for this modest deviation from circularity, there is significant power in the frequencies $\nu_\phi \pm \nu_r$. The beating of the fundamental ν_ϕ with the radial frequency $\nu_r = (1/3)\nu_\phi = 95$ Hz gives the set of secondary peaks at $(2/3)\nu_\phi$ and $(4/3)\nu_\phi$. Additional peaks occur at beats of the harmonic frequencies $n\nu_\phi \pm \nu_r$. It is interesting to note that there is not significant power in the radial mode at $\nu = 95$ Hz, but only in the beats with the fundamental azimuthal frequency and its harmonics. However, in the limit of a face-on orientation ($i \rightarrow 0^\circ$), the radial frequency should dominate the light curve variation as the gravitational and transverse Doppler red-shift modulate the intensity as a function of the hot spot’s radial coordinate. The radial mode should also be present in the limit of an edge-on orientation ($i \rightarrow 90^\circ$), as gravitational lensing becomes more important, and the hot spot will experience more magnification when closer to the black hole.

Figure 12 shows the dependence on inclination of the lower order harmonic and beat modes. At low inclinations, the radial frequency ($\nu/\nu_\phi = 1/3$) contributes significant power, while at higher inclinations, the first harmonic of the azimuthal mode begin to dominate with similar behavior to the circular orbits shown in Figure 9. Along with increasing power at $2\nu_\phi$, there is also increasing power in the radial beats of the first harmonic at $2\nu_\phi \pm \nu_r = (5/3)\nu_\phi, (7/3)\nu_\phi$. For a $10M_\odot$ black hole, all these frequencies should be observable within the timing sensitivity of RXTE.

To further explore the constraints of our model, we investigated the effect of orbital eccentricity on the QPO power. Maintaining a 1:3 commensurability between radial and azimuthal frequencies, we calculated the light curves for a range of eccentricities $0 \leq e \leq 0.2$. As expected, the beat modes at $\nu = \nu_\phi \pm \nu_r$ have more power for more eccentric orbits, as the radial variation of the emitter becomes larger. At the same time, the first harmonic

at $\nu = 2\nu_\phi$ provides relatively less power with increasing eccentricity. This is best understood as the “picket fence” character of the light curve becomes modulated in amplitude and frequency from peak to peak, i.e. for each 3-peak cycle, the time between peaks 1-2, 2-3, and 3-1 are not all the same, damping the harmonic overtone. Interestingly, the Fourier power in the beat modes appears to saturate at a moderate eccentricity of $e \approx 0.1$, suggesting highly eccentric geodesics are not necessary or even helpful for producing power in the beat frequencies.

While there is significant evidence for higher frequency harmonic and beat modes in the QPO power spectrum of XTE J1550-564, the Fourier power is clearly dominated by the two frequencies 184 and 276 Hz (Remillard et al. 2002), corresponding to $\nu_\phi - \nu_r$ and ν_ϕ in our model. What are the physical mechanisms that could damp out the higher frequency modes? One possible explanation is in the geometry of the hot spot. As explained in Section 4, in order to produce the power observed in QPOs, the relative flux coming from the hot spot must be some finite fraction of that of the disk (typically $10^{-3} - 10^{-2}$ for a QPO amplitude of 1 – 5%), so the hot spot must have some minimum size or it would not produce enough emission to be detected above the background disk. Yet if the hot spot is too large, it would be sheared by differential rotation in the accretion disk and not survive long enough to create the coherent X-ray oscillations that are observed. As mentioned above, we find that the relative QPO power in different modes is not sensitive to the size of the hot spot R_{spot} . Three-dimensional MHD simulations (Hawley & Krolik 2001) show a range of density and temperature fluctuations consistent with the hot spot size and over-brightness factor predicted by our model in conjunction with the observations.

It also appears from simulations that as the hot spot is formed in the disk, differential rotation will tend to shear a finite region of gas as it follows a geodesic orbit around the black hole, modifying the shape of the hot spot into an arc in azimuth. In the limit that the emission region could be sheared into a ring of arc length $\Delta\phi = 360^\circ$, the fundamental mode and its harmonics would be essentially removed, leaving power only in the radial modulation. Indeed, as shown in Figure 13a, for an arc length of $\Delta\phi = 180^\circ$, the higher frequency modes at $\nu = 2\nu_\phi$ and $\nu = 2\nu_\phi \pm \nu_r$ are strongly suppressed, while still maintaining a significant amount of power in the fundamental beat modes $\nu_\phi \pm \nu_r$. The total QPO power also increases as the area of the emission region increases relative to the circular hot spot geometry.

However, when we allow the arc to be sheared into a ring with $\Delta\phi = 360^\circ$, the total QPO power is actually decreased as the differential beaming is essentially eliminated by the extended emission region: there is always some portion of the arc moving toward the observer. The resulting modulation is then more weighted to the first radial beat mode at $\nu_\phi - \nu_r$, as seen in Figure 13b. It is not intuitively obvious why the $\nu_\phi - \nu_r$ mode is dominant while the $\nu_\phi + \nu_r$ mode ($\nu = 368$ Hz) is much weaker in the arc geometry. If anything, this is a strong argument for the necessity of a full ray-tracing calculation of the hot spot light curves when predicting QPO power spectra, as it clearly gives information unavailable to simple analysis

of the geodesic coordinate frequencies.

This behavior offers a plausible explanation for the two major types of QPOs described in Remillard et al. (2002). Type A outbursts have more total power in the HFQPOs, with a major peak at 276 Hz and a minor peak at 184 Hz. Type B outbursts have most of the QPO power around 184 Hz and a smaller peak around 276 Hz and less overall power in the high frequency region of the spectrum. Thus we propose that Type A outbursts are coming from more localized hot spot regions, while Type B outbursts come from a more extended ring geometry.

In addition to the commensurate high-frequency QPOs observed in sources like XTE J1550-564, there are also strong low-frequency QPOs observed at the same time with frequencies in the range 5 – 15Hz. There have been suggestions that these low-frequency QPOs may be caused by the Lens-Thirring precession of the disk near the ISCO, also known as “frame dragging” (Markovic & Lamb 1998; Merloni, Vietri, & Stella 1999; Abramowicz & Kluzniak 2001; Remillard et al. 2002). For geodesic orbits out of the plane perpendicular to the black hole spin, the latitudinal frequency Ω_θ of massive particles is not equal to the azimuthal frequency Ω_ϕ [see eqs. (24) and (18)], leading to a precession of the orbital plane with frequency

$$\Omega_{LT} \equiv |\Omega_\theta - \Omega_\phi|. \quad (28)$$

For black holes with the mass and spin used above ($M = 10M_\odot$, $a/M = 0.5$), the frame-dragging frequency, as calculated at the radius corresponding to the commensurability $\nu_r:\nu_\phi=1:3$, is somewhat higher than that observed in the low-frequency QPOs from XTE J1550-564. The Type A QPO peaks at 12 and 276 Hz appear to be consistent with a black hole mass of $8.9M_\odot$ and spin parameter of $a/M = 0.35$, quite similar to the values used throughout much of this paper. For the BH binary GRO J1655-40, we can fit the QPOs at 18 and 450Hz with a mass of $5.1M_\odot$ and spin $a/M = 0.28$, slightly less than the published mass range of $5.5 - 7.9M_\odot$ (Shahbaz et al. 1999). If we relax the requirement of matching the LFQPOs and only fit the HFQPOs with a 1:3 coordinate frequency commensurability, there remains a 1-dimensional degeneracy in the mass-spin parameter space. Based solely on the HFQPOs, for XTE J1550-564 with $8.5 < M/M_\odot < 11.5$, the range of spin parameters would be $0.33 < a/M < 0.6$ and for GRO J1655-40, the spin would be in the range $0.35 < a/M < 0.66$. These results are shown in Table 1.

To get a more quantitative feeling for the effect of Lens-Thirring precession on the power spectrum, we investigated hot spot orbits with initial trajectories inclined to the plane of the disk: $v^\theta \neq 0$. This is much like changing the observer’s inclination with a period of $2\pi/\Omega_{LT}$. Thus we see additional modulation in the hot spot light curve at the “double-beat” modes $\nu_\phi \pm \nu_r \pm \nu_{LT}$. We find that, for modestly inclined hot spot orbits ($i_0 = \pm 5^\circ$), the contribution to the power spectrum at Lens-Thirring frequencies is quite small ($< 1\%$ of total power) for the basic circular hot spot geometry. This relative contribution increases with arc length as the spot becomes a ring precessing about the spin axis, consistent with the relative power in LFQPOs and HFQPOs in the Type A (more high frequency power than low frequency) and Type B (more low frequency power) sources described above.

Under the premise that the HFQPO commensurate fre-

quencies are caused by the geodesic motion of a sheared, overbright region in the disk, in Table 2 we show the best fit parameters for the Type A and Type B QPO spectra from XTE J1550-564 [cf. Table 1 in Remillard et al. (2002)]. Guided also by the (somewhat speculative) assumption that the LFQPOs come from the Lens-Thirring precession of the hot spot orbital plane, we predict a black hole mass and spin. Using a fixed inclination of 70° , we can match the frequencies and amplitudes of the observed HFQPO peaks (and, equally important, the lack of power at certain frequencies) for both Type A and Type B outbursts. Setting constant the eccentricity $e = 0.1$, geodesic inclination to the disk $i_0 = 5^\circ$, and the overbrightness to be a factor of unity, we fit the hot spot radius and arc length to match the observations. Being able to match the QPO rms amplitudes of the peaks (or lack thereof) at 92, 184, 276, and 368 Hz, for at least two different types of X-ray outburst, shows the robustness of our simple model in explaining these phenomena.

However, even with the sheared arc emission, many observations still show significantly more power in the LFQPOs than can be explained solely from the Lens-Thirring precession of a geodesic near the ISCO. Coupled with the difficulty in simultaneously fitting the mass and spin to three coordinate frequencies in a manner consistent with spectroscopic mass predictions, it seems likely that the LFQPOs may be caused by some other mechanism in the disk that is related only indirectly to the high-frequency hot spot emission. Another possibility is that the thin, warped disk model breaks down near the ISCO, allowing more complicated emission geometries and thus amplifying the effects of Lens-Thirring precession.

6. CONCLUSIONS

We have developed a hot spot model to help understand the high-frequency QPOs observed in accreting black holes. While the model does not consider radiation or hydrodynamic pressures, it is fully relativistic and calculates exact geodesics for both massive particles and photons. Treating the hot spot as a monochromatic, isotropic emitter, we have calculated the time-dependent spectra of X-ray lines produced as the hot spot orbits the black hole.

The model makes a number of general predictions of the Fourier power of the X-ray light curve as a function of inclination and black hole spin, and is also able to explain QPO observations from the black hole binaries XTE J1550-564 and GRO J1655-40. Simply by matching the locations of the low-frequency and high-frequency QPOs with the coordinate frequencies (under the condition $\nu_\phi = 3\nu_r$), we can determine the black hole mass and spin. Relaxing the LFQPO constraint, the spin can still be determined uniquely for a given mass, which in turn can often be measured independently with the inclination and radial velocity of the companion star.

By matching the amplitudes of various peaks observed in XTE J1550-564, we have explored the model parameters such as the hot spot size, shape, and the overbrightness relative to a steady-state background disk. The predicted magnitude of these fluctuations are within the range predicted by 3D MHD calculations of the accretion disk. Future work will investigate the effect of multiple hot spots of various size, emissivity, and lifetime, as guided by MHD

calculations. Observations of additional sources with commensurate frequency QPOs may help us further constrain the hot spot model and better understand the connection between the LFQPOs and HFQPOs.

Some of the physical problems with the hot spot model have been raised by Markovic & Lamb (2000), as discussed above. Many of these points are addressed in our model. First, unlike Stella & Vietri (1998, 1999), we only attempt to explain a set of QPO data from *black hole* binaries, which differ qualitatively from neutron star binaries in many ways, e.g. lacking strong global magnetic fields and thermonuclear activity. And perhaps most significant, black holes have no rotating surface to interact with the accreting matter and provide additional confusion to the QPO power spectrum. Our model produces light curves with power spectra consistent with black hole observations even with low eccentricity hot spot orbits.

Because they do not include ray tracing in their calculations, Markovic & Lamb (2000) are unable to model many relativistic effects, including the gravitational lensing of the hot spot source, which can be quite significant for systems with moderate to high inclination angles ($i \geq 60^\circ$). Since we calculate the actual X-ray modulation from the orbiting hot spots, we predict both the location and amplitude of every peak in the light curve power spectrum, which cannot be done by analyzing the BH coordinate frequencies alone. By introducing a perturbation on circular orbits near the ISCO, additional peaks begin to appear in the power spectrum, caused by beats of the azimuthal and radial frequencies ν_ϕ and ν_r . The dependence of the relative power in the different peaks on inclination and spin helps to constrain the details of the hot spot model in explaining the HFQPOs, particularly the 2:3 commensurability observed in the power spectra from XTE J1550-564 and GRO J1655-40.

As an additional parameter, we introduce a finite arc length for the emission region, motivated by the shearing of the hot spot by differential rotation in the disk. The spreading of the hot spot in azimuth leads to suppression of the higher QPO modes, in agreement with observations. We have also examined the possibility of Lense-Thirring precession for non-planar orbits as an explanation for the low-frequency QPOs that have been observed coincident with the HFQPOs yet often with even stronger Fourier power. The predicted power spectra from non-planar precessing arcs are consistent with observations of XTE J1550-564 if we associate Type A outbursts with hot spot arcs of $\Delta\phi \approx 180^\circ$ and Type B outbursts with hot spot rings of $\Delta\phi \approx 360^\circ$. However, the difficulty in matching the LFQPOs amplitude and frequency with a single hot spot geodesic suggests the low-frequency modulations may be caused by a different mechanism or perhaps our disk geometry is too simplistic.

One major remaining issue with the hot spot model is the preferred location of the geodesic that gives rise to 1:3 coordinate frequencies. Why should the orbital frequencies favor integer ratios, and why should the preferred ratio be 1:3 and not 1:2 or 1:4? It is possible that detailed radiation-hydrodynamic calculations with full general relativity will be required to answer this question. Perhaps the non-circular orbits can only survive along closed orbits such as these to somehow avoid destructive intersec-

tions. Or there may be magnetic interactions with the black hole itself, analogous to the Blandford-Znajek process, that lock the accreting gas into certain preferred trajectories (Wang et al. 2003). For now, we are forced to leave this as an open question unanswered by the geodesic hot spot model.

A less difficult, yet still unanswered problem is the explanation of the widths of the QPO peaks. As it stands, our hot spot model predicts purely periodic light curves and thus power spectra made up of delta functions. If there *is* some physical mechanism that preferentially focuses accreting material onto eccentric orbits at specific radii, then it is likely that these hot spots are forming and then being destroyed as a continual processes. The superposition of many hot spots around the same orbit, all with slightly different initial trajectories, could explain the quasi-periodic nature of the power spectrum: the phase decoherence of the hot spots would cause a natural broadening of the strictly periodic signal from a single spot. With the computational framework in place, this question can be answered by modeling a whole collection of hot spots and arcs continually forming and evolving in shape and emissivity. The particular physical parameters for these hot spots can be derived from published MHD calculations such as Hawley & Krolik (2001). With the basic ray-tracing and radiation transport methods in place, it should be possible to use our code as a “post-processor” to analyze the results of these 3D simulations to simulate X-ray light curves and spectra from a realistic accretion disk.

A final piece of the black hole QPO puzzle is the spectral behavior of the source during outburst. Remillard et al. (2002) have shown there is a large range of X-ray fluxes with different relative contributions from a power-law component and a disk bolometric component. These relative and absolute fluxes seem to be correlated with the amount of power in both the LFQPOs and the HFQPOs. Future work on 3-dimensional disks and more detailed radiative transfer models should give us important insights into understanding this spectral behavior and its relation to the QPO power.

We thank Ron Remillard and Mike Muno for helpful discussion and comments on the manuscript. This work was supported by NASA grant NAG5-13306.

REFERENCES

- Abramowicz, M. A., & Kulznik, W. 2001, *A&A*, 375, L19
 Abramowicz, M. A., et al. 2002, preprint (gr-qc/0202020)
 Abramowicz, M. A., et al. 2003, *PASJ*, in press (astro-ph/0302183)
 Armitage, P. J., Reynolds, C. S., & Chiang, J. 2001, *ApJ*, 548, 868
 Bao, G. 1992, *Astron. & Astro.* 257, 594
 Bardeen, J. M., Press, W. H., Teukolsky, S. A. 1972, *ApJ*178, 347
 Blandford, R. D., & Znajek, R. L. 1977, *MNRAS*, 179, 433
 Bromley, B. C., Chen, K., & Miller, W. A. 1997, *ApJ*, 475, 57
 Carter, B. 1968, *Phys. Rev. Lett.* 26, 331
 Ford, E. C. 2000, *ApJ*535, L119
 Ford, E. C. et al. 2000, *ApJ*539, 368
 Ghosh, P., & Lamb, F. K. 1978, *ApJ*, 223, L83
 Gierlinsky, M., Done, C., Barret, D. 2002, *MNRAS* 331, 141
 Hawley, J. F., & Krolik, J. H. 2001, *ApJ*, 548, 348
 Karas, V., Vokrouhlicky, D., & Polnarev, A. G. 1992, *MNRAS*, 259, 569
 Kojima, Y. 1991, *MNRAS* 250, 629
 Kluzniak, W., & Abramowicz, M. A. 2001, preprint (astro-ph/0105057)
 Kluzniak, W., & Abramowicz, M. A. 2002, preprint (astro-ph/0206063)
 Lamb, F. K. 2002, in *X-ray Binaries and Gamma-Ray Bursts*, ed. E. P. J. van den Heuvel (San Francisco: Astronomy Society of the Pacific)
 Lanzafame, G., Molteni, D., & Chakrabarti, S. K. 1998, *MNRAS*, 299, 799
 Laor, A. 1991, *ApJ*, 376, 90
 Lee, W. H., & Ramirez-Ruiz, E. 2002, *ApJ*, 577, 893
 Markovic, D., & Lamb, F. K. 1998, *ApJ*, 507, 316
 Markovic, D., & Lamb, F. K. 2000, preprint (astro-ph/0009169)
 Merloni, A., Vietri, M., Stella, L., & Bini, D. 1999, *MNRAS*, 304, 155
 Miller, J. M. et al. 2002, *ApJ*, 570, L69
 Misner, C. W., Thorne, K. S., & Wheeler, J. A. 1973, *Gravitation* (New York: W. H. Freeman)
 Pariev, V. I., Bromley, B. C., Miller, W. A. 2001, *ApJ*, 547, 649
 Rauch, K. P., & Blandford, R. D. 1994, *ApJ*, 421, 46
 Remillard, R. A. et al. 2002, *ApJ*, 580, 1030
 Reynolds, C. S., & Begelman, M. C. 1997, *ApJ*, 488, 109
 Shahbaz, T., et al. 1999, *MNRAS*, 306, 89
 Shakura, N. I., & Sunyaev, R. A. 1973, *Astron. Astrophys.*, 24, 337
 Shapiro, S. L., & Teukolsky, S. A. 1983, *Black Holes, White Dwarfs, and Neutron Stars* (New York: John Wiley & Sons, Inc.)
 Stella, L., & Vietri, M. 1998, *ApJ*, 492, L59
 Stella, L., & Vietri, M. 1999, *Phys. Rev. Lett.*, 82, 17
 Strohmayer, T. E. 2001, *ApJ*, 552, L49
 Strohmayer, T. E. 2001, *ApJ*, 554, L169
 Wagoner, R. V., Silbergleit, A. S., & Ortega-Rodriguez, M. 2001, *ApJ*, 559, L25
 Wang, D. X. 2003, *MNRAS*, in press (astro-ph/0305478)

TABLE 1

BLACK HOLE PARAMETERS FOR HOT SPOT MODEL, MATCHING LOW-FREQUENCY AND HIGH-FREQUENCY QPOs TO GEODESIC COORDINATE FREQUENCIES

Black Hole Parameters	XTE J1550-564	GRO J1655-40
BH Mass	$8.9M_{\odot}$	$5.1M_{\odot}$
BH Spin	$0.35M$	$0.28M$
R_{ISCO}	$4.8M$	$5.05M$
Inclination	70°	65°
<hr/>		
Geodesic Frequencies		
r_0	$5.54M$	$5.77M$
ν_{LT}	12 Hz	17 Hz
ν_r	92 Hz	150 Hz
ν_{ϕ}	276 Hz	450 Hz

TABLE 2

QPO AMPLITUDES OF HOT SPOT/ARC MODEL FOR XTE J1550-564

Parameter	Type A	Type B	
R_{spot}	$0.3M$	$0.5M$	
arc length	200°	320°	
eccentricity	0.1	0.1	
inclination to disk	5°	5°	
overbrightness	100%	100%	
Amplitude (mode)	Frequency (Hz)	rms(%)	rms(%)
$a(\nu_{\text{LT}})$	12	0.63	2.1
$a(\nu_r)$	92	0.48	0.89
$a(\nu_{\phi} - \nu_r)$	184	1.3	2.2
$a(\nu_{\phi})$	276	3.2	0.42
$a(\nu_{\phi} + \nu_r)$	368	0.20	0.23

FIG. 1.— Schematic picture of ray-tracing method from distant observer through a disk of angular thickness $\Delta\theta$. The rays either terminate at the black hole horizon or pass through the disk, with each point of intersection labeled with the photon position and momentum (x^μ, p_μ) .

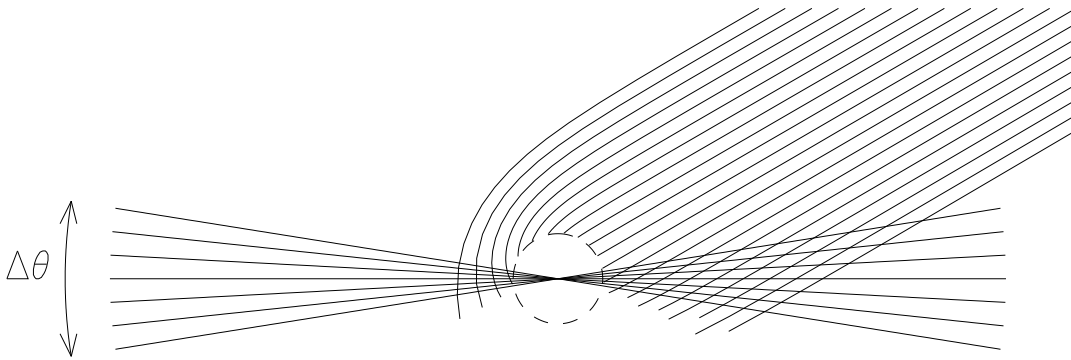


FIG. 2.— Projection of a uniform Cartesian grid in the image plane onto the source plane of the accretion disk ($\theta = \pi/2$). Inclination angles are $i = 0^\circ$ (*top*) and $i = 60^\circ$ (*bottom*) and spin parameters are $a/M = 0$ (*left*) and $a/M = 0.95$ (*right*). The region inside the horizon is cut out from each picture.

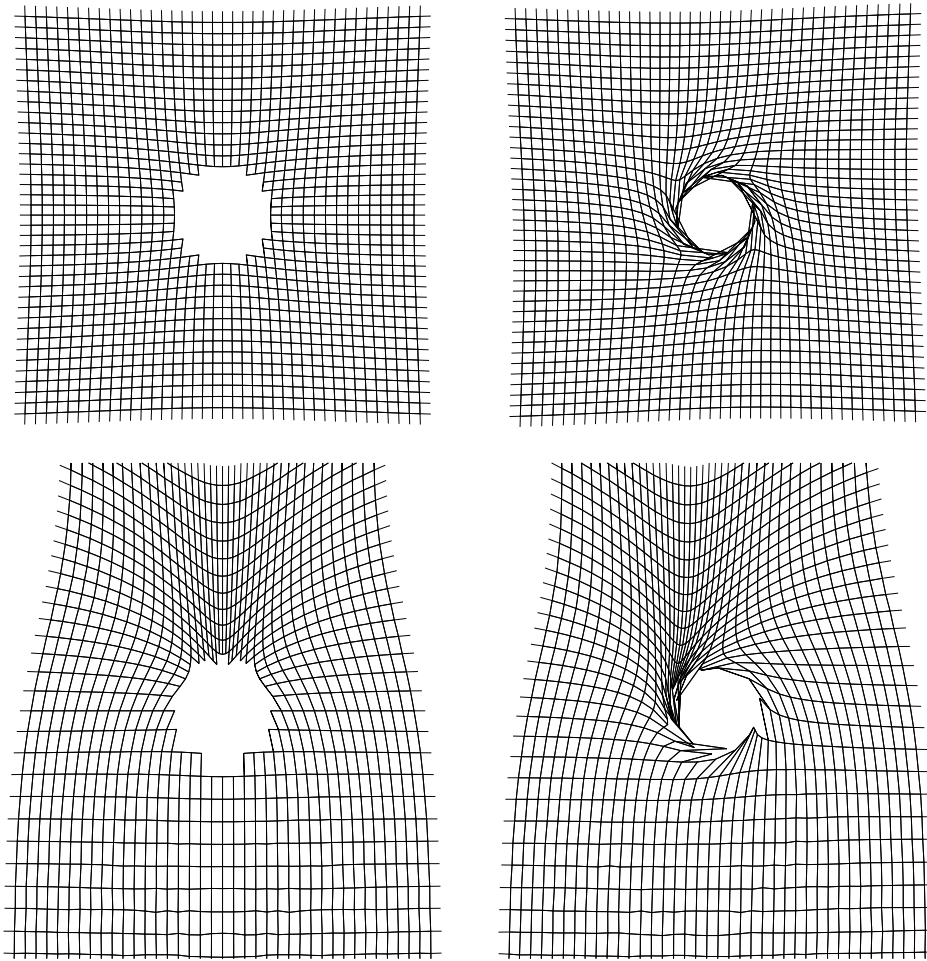


FIG. 3.— Normalized spectra of a monochromatic emission line from steady-state accretion disks of varying inclination. An inclination of $i = 0^\circ$ corresponds to a face-on view of the disk while $i = 90^\circ$ would be edge-on. The emissivity is taken to be uniform between $R_{\text{in}} = R_{\text{ISCO}}$ and $R_{\text{out}} = 15M$. The spin is taken to be $a/M = 0.5$ but the dependence on a is negligible for uniformly emitting disks.

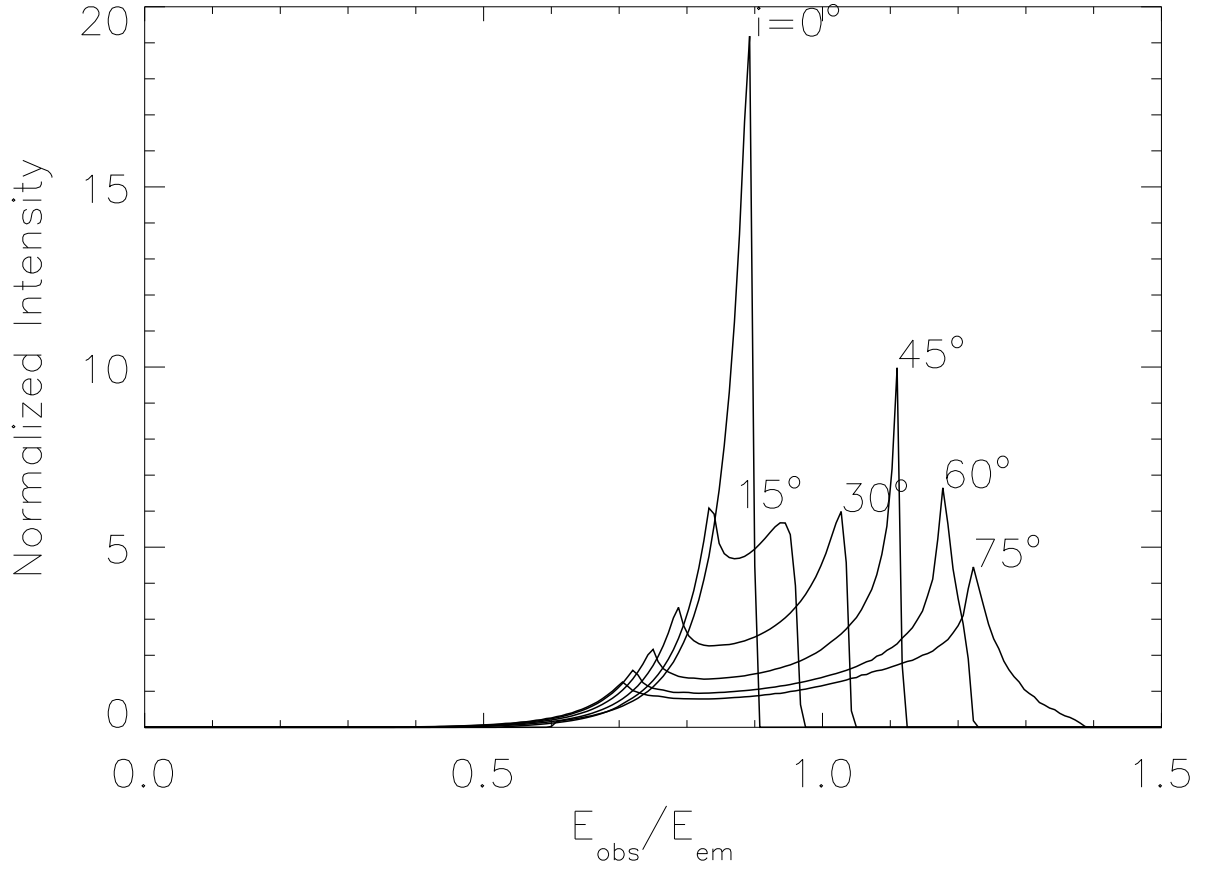


FIG. 4.— Normalized spectra of steady-state accretion disks with inclination $a = 30^\circ$ and varying spin parameter a (negative values of a correspond to retrograde disk rotation). The emissivity is taken to be proportional to r^{-2} between $R_{\text{in}} = R_{\text{ISCO}}$ and $R_{\text{out}} = 15M$. Black holes with higher values of a allow the inner disk to extend in closer to the horizon, giving a greater weight to the high-redshift radiation emitted there.

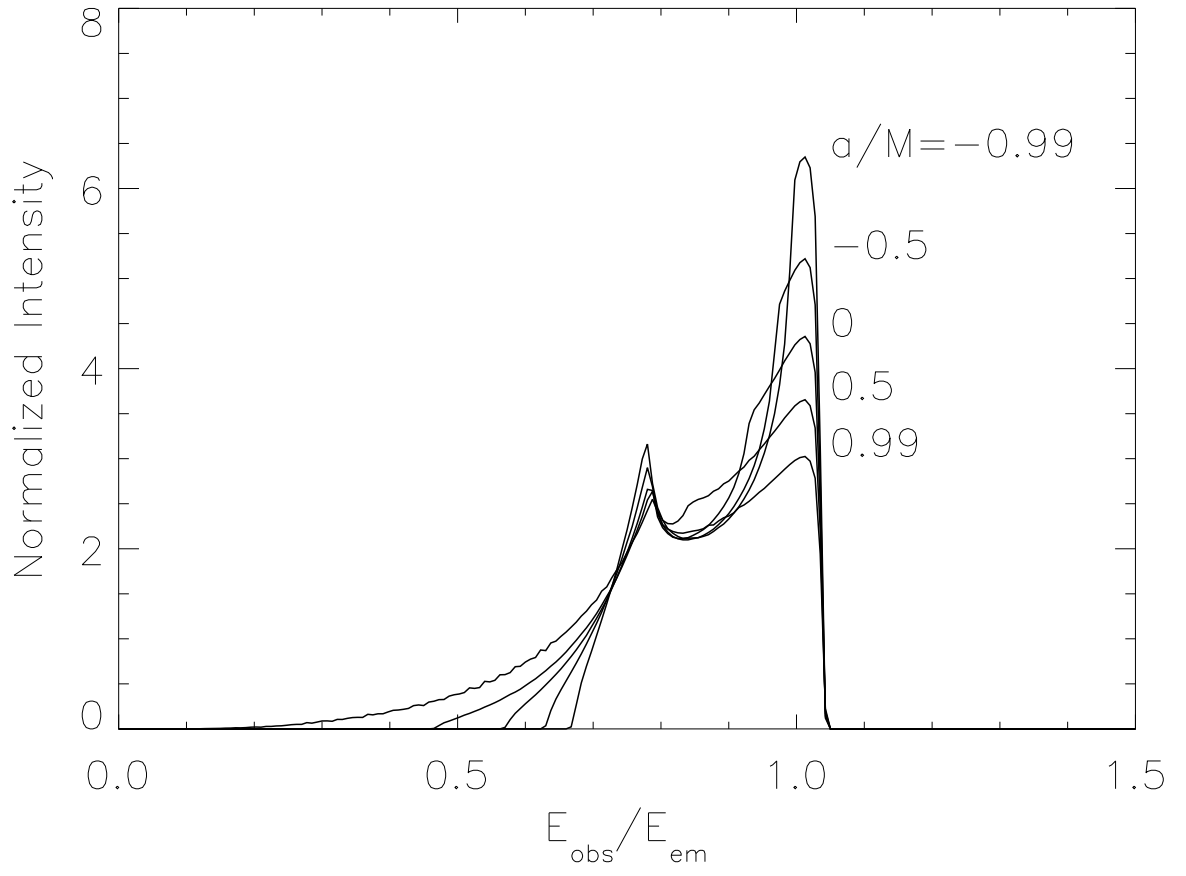


FIG. 5.— Spectrogram of a circular hot spot with radius $R_{\text{spot}} = 0.5M$ orbiting a Schwarzschild black hole at the ISCO ($R_{\text{ISCO}} = 6M$), viewed at an inclination of 60° . The spot is moving in the $-\mathbf{e}_{\hat{\phi}}$ direction with the observer at $\phi = 270^\circ$. The maximum redshift occurs when $\phi \approx 160^\circ$ and the maximum blueshift occurs when $\phi \approx 20^\circ$.

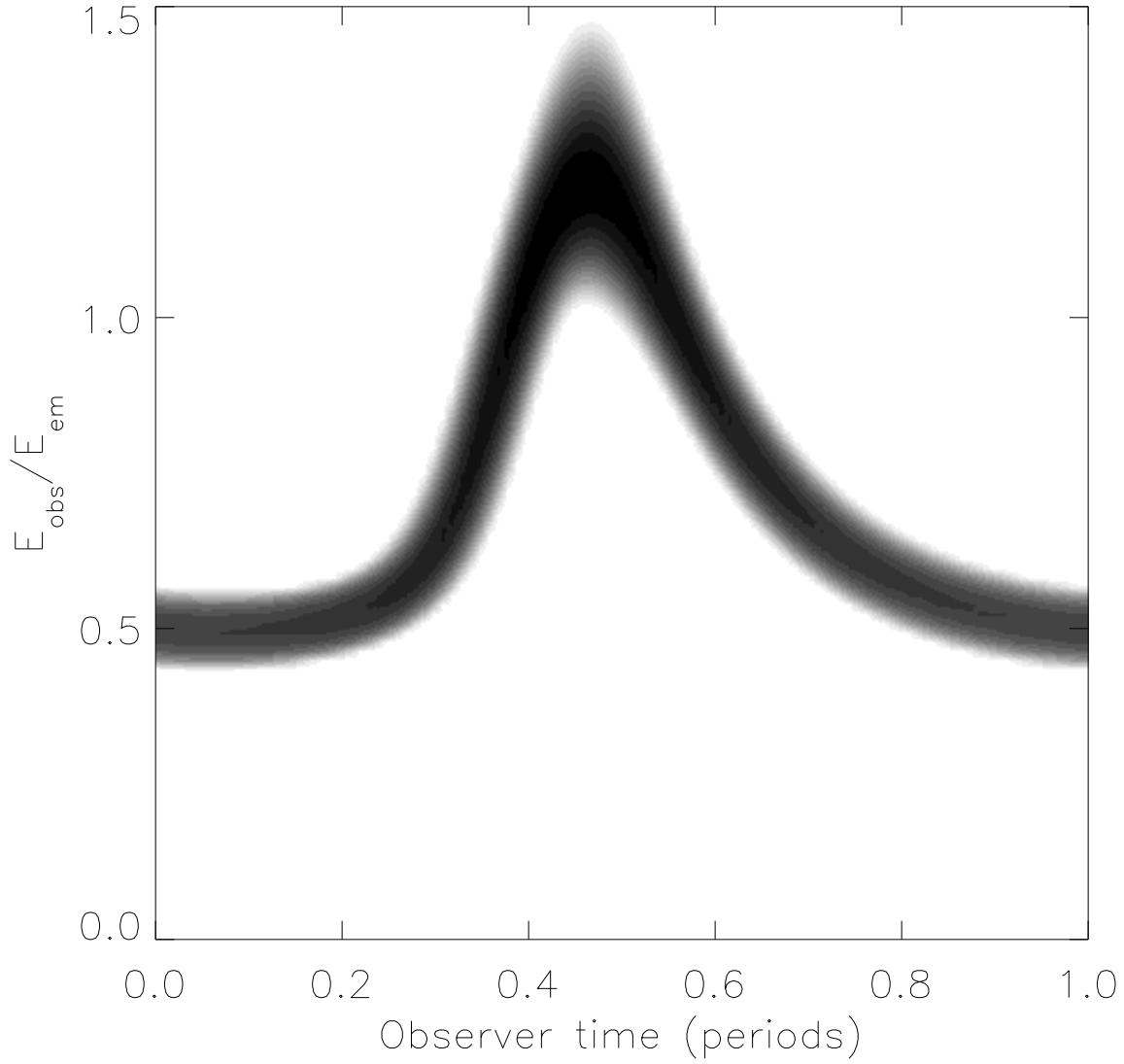


FIG. 6.— Overbrightness required of a hot spot on a circular orbit to produce a 1% rms modulation in X-ray flux when added to a steady-state disk with $R_{\text{in}} = R_{\text{ISCO}}$, $R_{\text{out}} = 15M$ and emissivity $g(r) \propto r^{-2}$. An overbrightness of unity means the peak hot spot emissivity is twice that of the steady-state disk with no hot spot. The spot size R_{spot} is measured in gravitational radii M , so for a black hole with $a/M = 0.5$ and $i = 60^\circ$, the required overbrightness for a hot spot with $R_{\text{spot}} = 0.5M$ would be 67%.

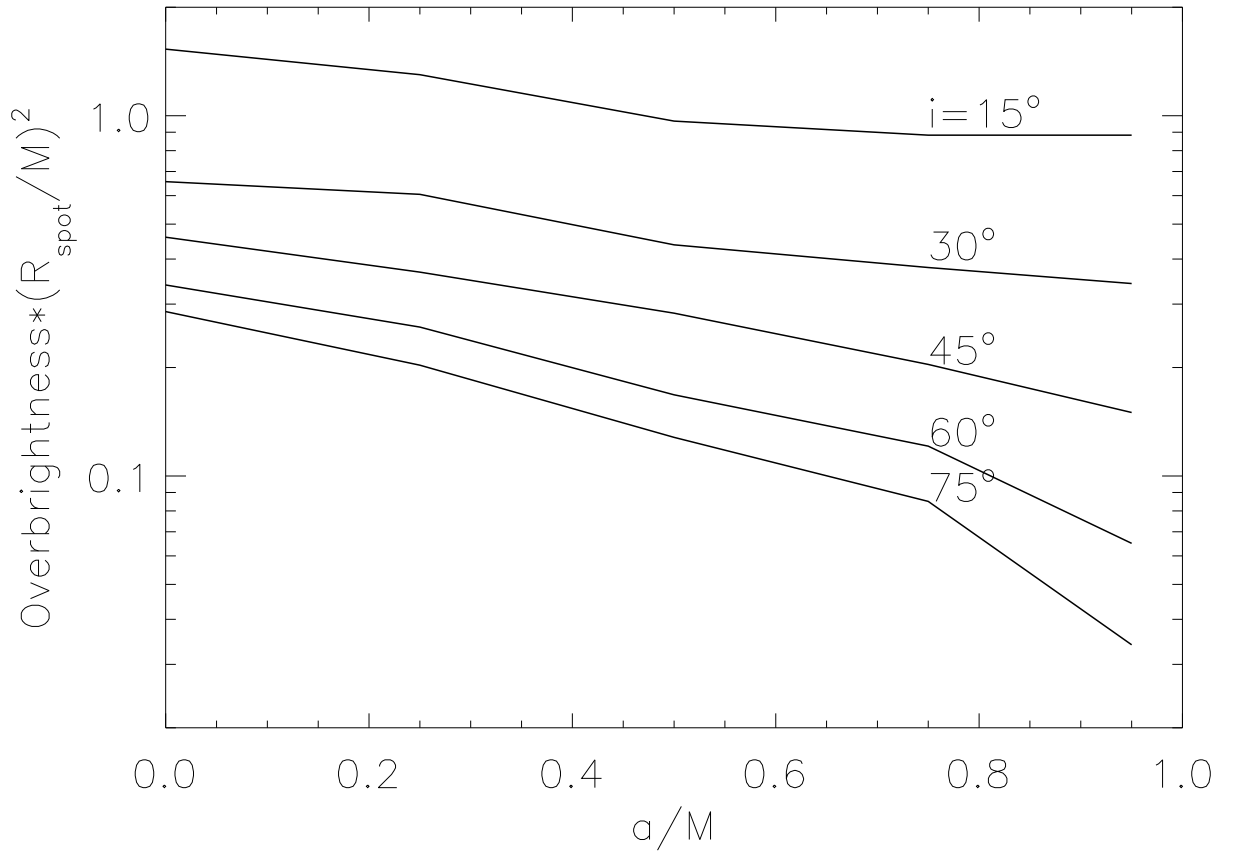


FIG. 7.— Frequency-integrated light curves of an orbiting hot spot at the ISCO of a Schwarzschild black hole for different disk inclination angles. The spot is moving in the $-\mathbf{e}_{\hat{\phi}}$ direction as in Figure 5. For high inclination angles, the special relativistic beaming causes the light curve to become sharply peaked as the hot spot moves toward the observer.

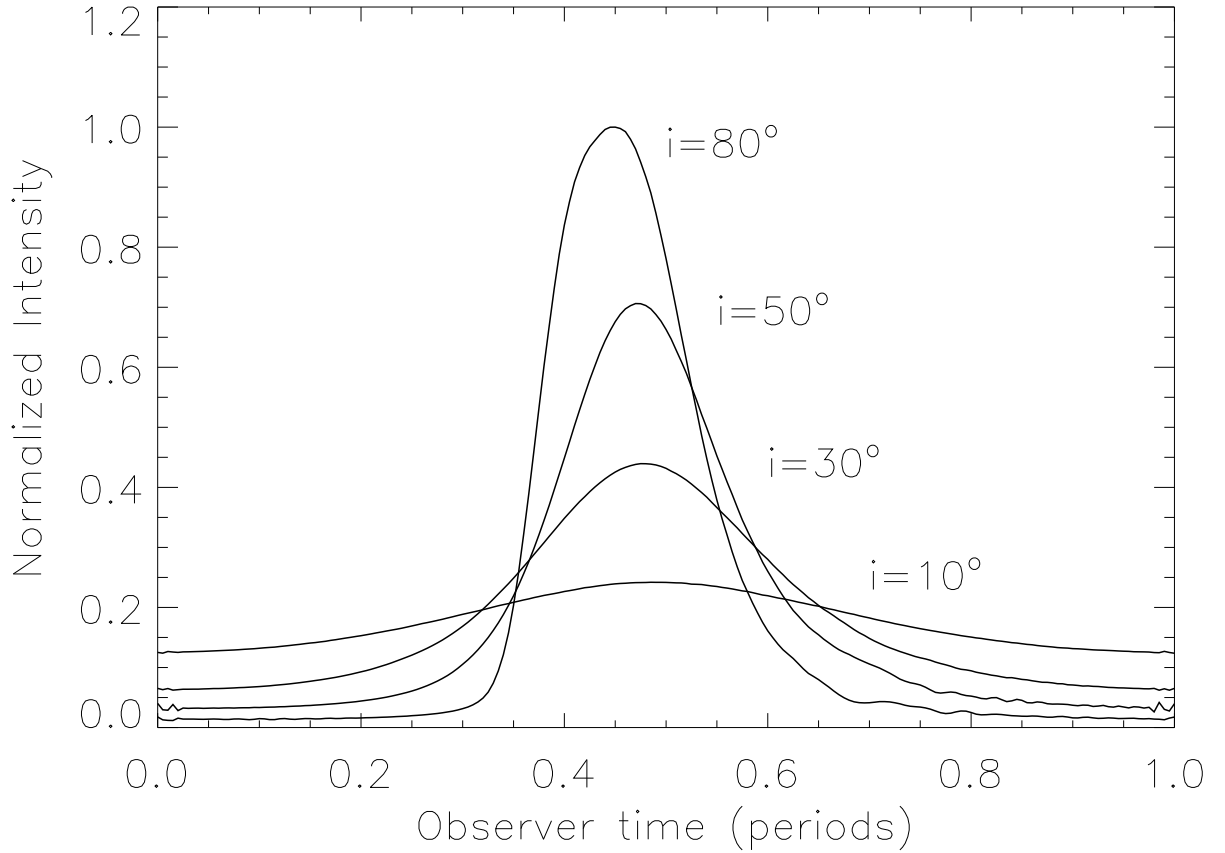


FIG. 8.— (a) X-ray light curve of an orbiting hot spot with same parameters as in Figure 5. (b) Fourier amplitude $a_n(\text{rms})$ of the above light curve with overbrightness of unity, normalized to the flux from a steady-state disk as in equation (22), showing the fundamental Kepler frequency at 220 Hz for $M = 10M_\odot$. The non-sinusoidal shape of the light curve, due largely to beaming effects, is characterized by the declining power in the higher harmonic frequencies at $n220$ Hz, where $n > 1$ is an integer.

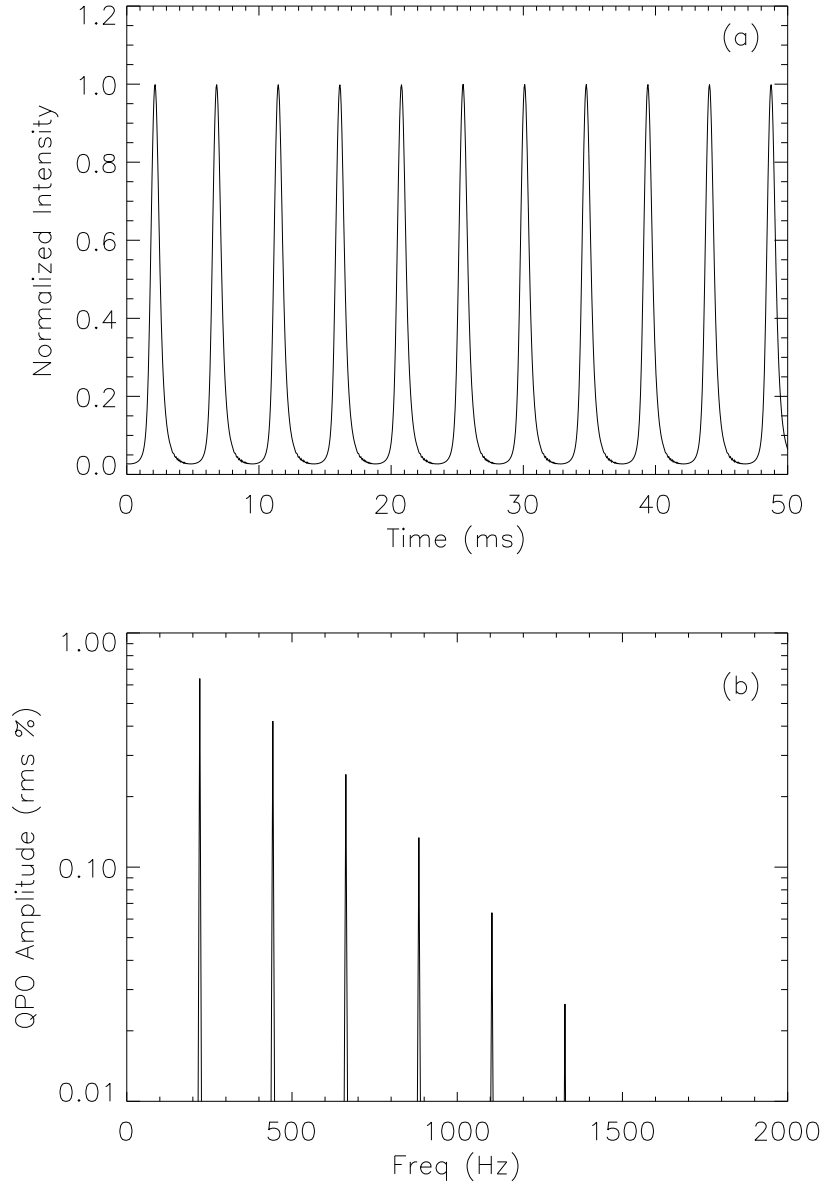


FIG. 9.— Fourier amplitude $a_n(\text{rms})$ in higher harmonic frequencies $\nu_n = n\nu_\phi$ as a function of orbital inclination to the observer, normalized as in equation (22). The hot spot has size $R_{\text{spot}} = 0.5M$, an overbrightness factor of 100%, and is in a circular orbit at R_{ISCO} around a Schwarzschild black hole.

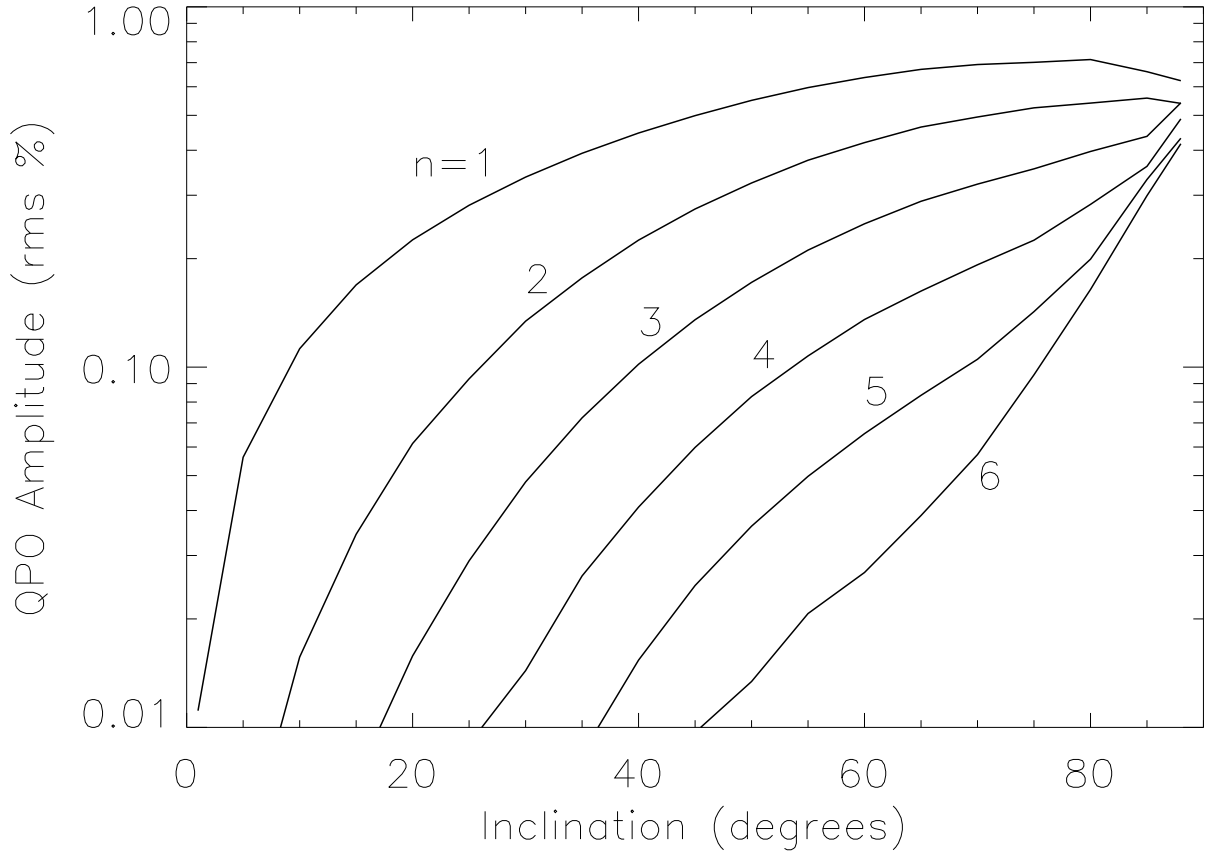


FIG. 10.— Radius of prograde orbits with commensurate frequencies $\nu_r : \nu_\phi = (1:3, 1:2, 2:3)$ (solid lines) as a function of dimensionless spin parameter a/M . The ISCO (dashed line) corresponds to $\nu_r : \nu_\phi = 1 : \infty$. Also shown are the respective orbital frequencies ν_ϕ at these radii for a black hole with mass $10M_\odot$ (dot-dashed lines).

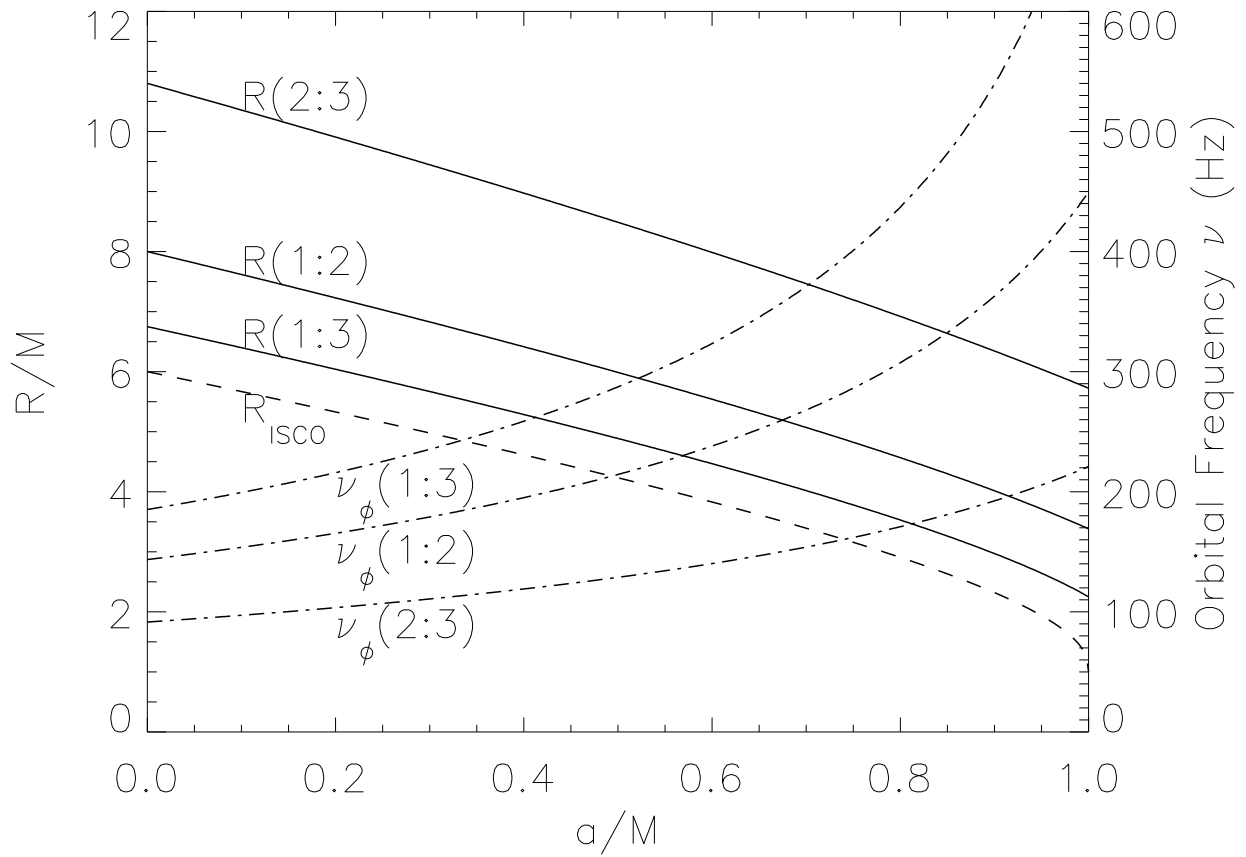


FIG. 11.— (a) X-ray light curve of a hot spot orbit with $\nu_\phi = 3\nu_r$, $e = 0.089$, $M = 10M_\odot$, $a/M = 0.5$, $i = 60^\circ$, and $R_{\text{spot}} = 0.5M$. (b) The Fourier amplitude $a_n(\text{rms})$ of the above light curve, normalized as in Figure 8b, showing the fundamental Kepler frequency at $\nu_\phi = 285$ Hz and beat modes at $\nu = n\nu_\phi \pm \nu_r$.

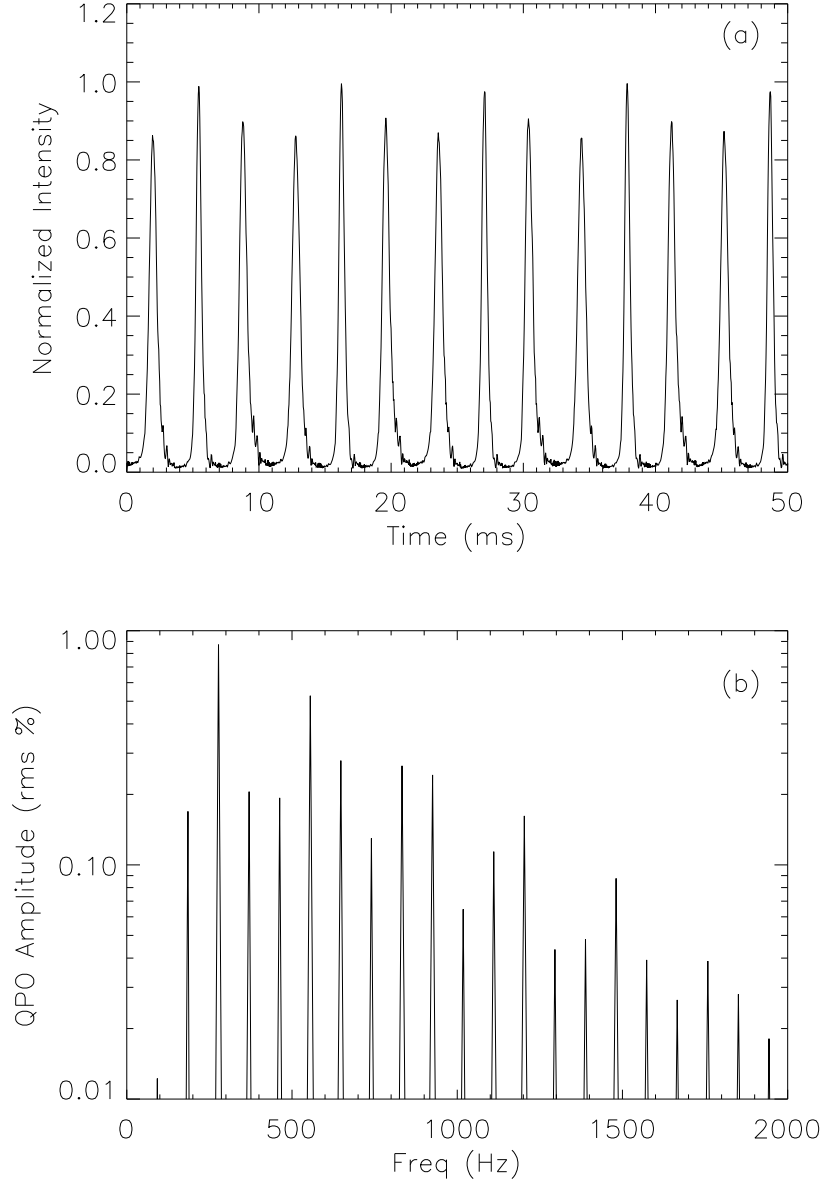


FIG. 12.— Power in low-order harmonics and beat modes with frequencies $\nu = n\nu_\phi \pm \nu_r$, as a function of disk inclination angle. The hot spot trajectory is the same as in Figure 11, with $a_n(\text{rms})$ normalized as in Figure 9. The curves are labeled by the ratio ν/ν_ϕ .

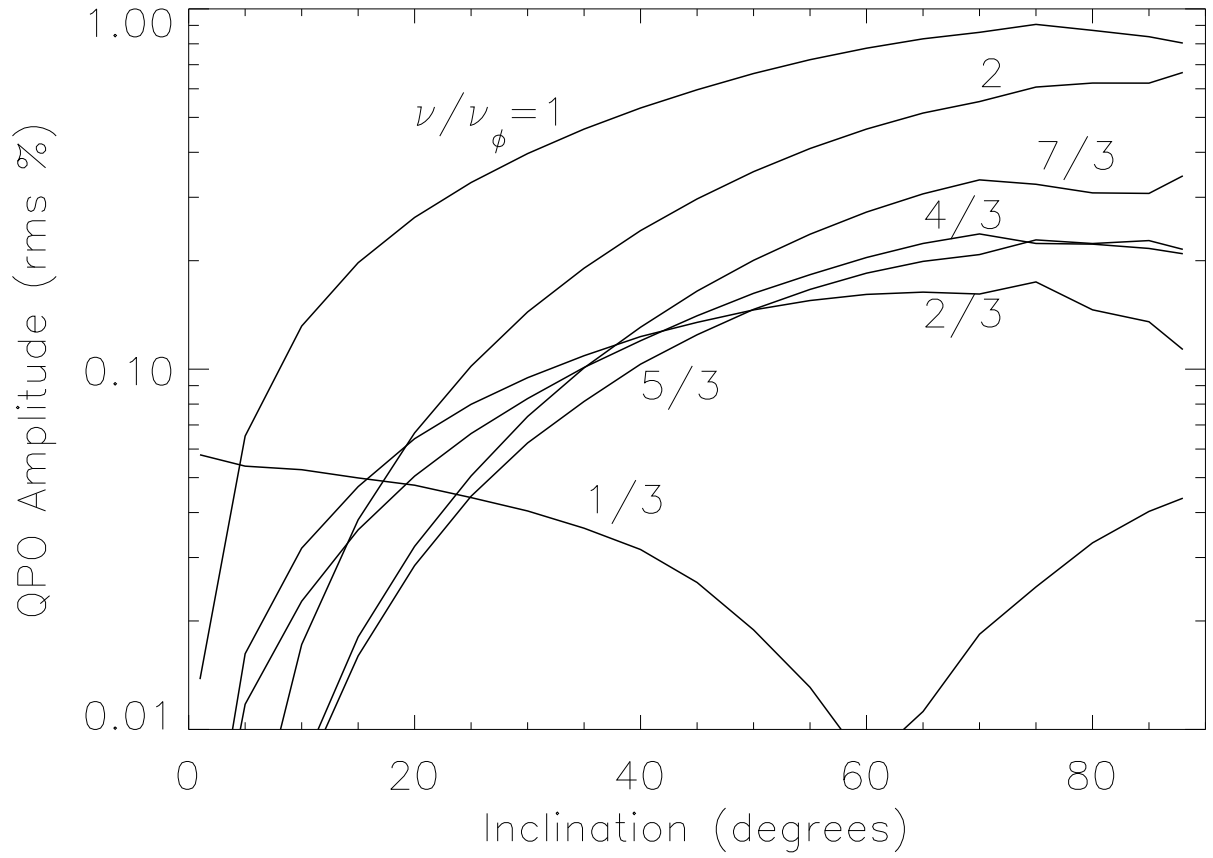


FIG. 13.— Power spectrum for a hot spot with same trajectory as in Figure 11, with the emission region sheared along the geodesic into an arc of length (a) 180° and (b) 360° . For the shorter arc (a), the power is still peaked at the fundamental frequency $\nu_\phi = 285$ Hz, while the extended arc (b) produces more power in the beat frequency $\nu_\phi - \nu_r = 190$ Hz.

